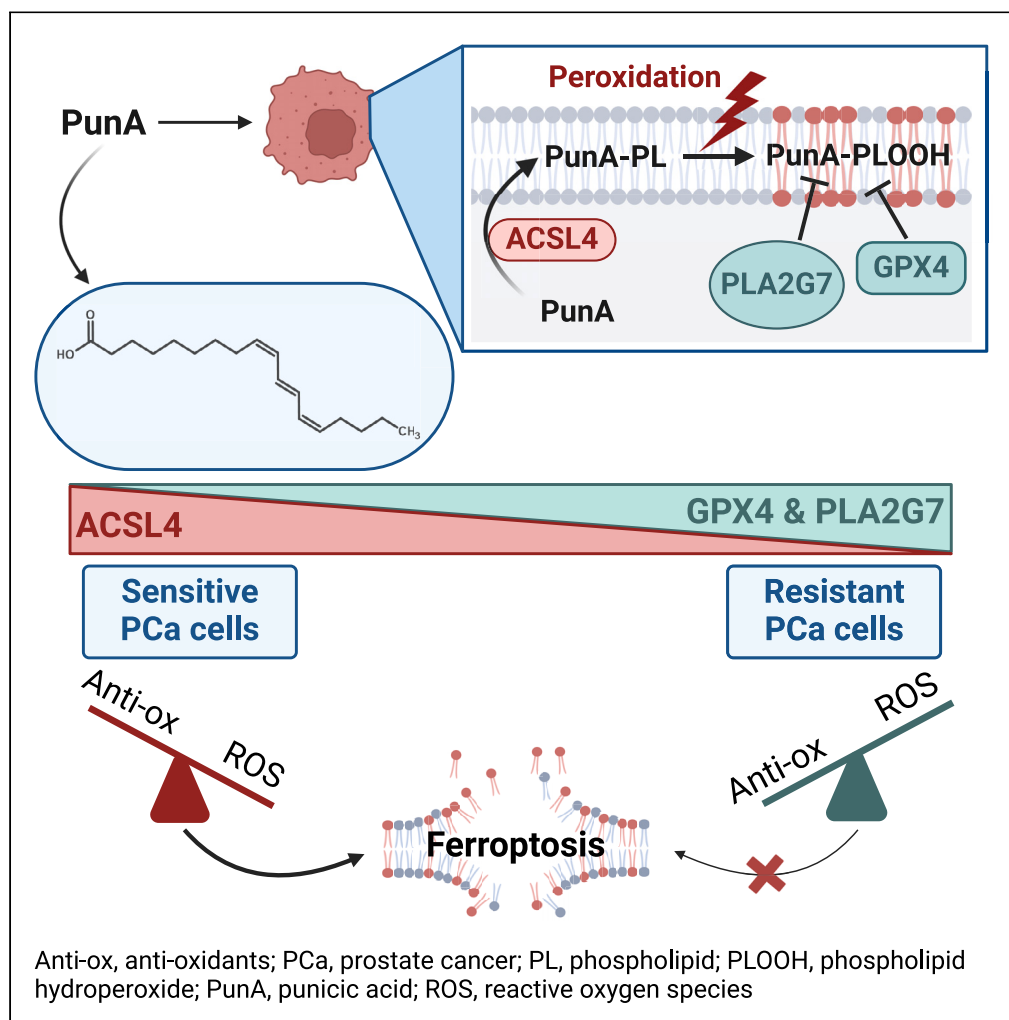


## Article

## Phospholipase PLA2G7 is complementary to GPX4 in mitigating punicic-acid-induced ferroptosis in prostate cancer cells



Perrine Vermonden, Manon Martin, Katarzyna Glowacka, ..., Cathy Debier, Olivier Feron, Yvan Larondelle

yvan.larondelle@uclouvain.be

## Highlights

Punicic acid (PunA) induces ferroptosis in prostate cancer cells (PCa)

PunA triggers a massive lipidome remodeling, notably in androgen-negative PCa cells

Phospholipase PLA2G7 is a suppressor of PunA-induced ferroptosis in PCa cells

PLA2G7 complements GPX4 in protecting PCa cells from PunA-induced ferroptosis

Vermonden et al., iScience 27, 109774  
May 17, 2024 © 2024 The Author(s). Published by Elsevier Inc.  
<https://doi.org/10.1016/j.isci.2024.109774>

## Article

## Phospholipase PLA2G7 is complementary to GPX4 in mitigating puniceic-acid-induced ferroptosis in prostate cancer cells

Perrine Vermondan,<sup>1</sup> Manon Martin,<sup>1</sup> Katarzyna Glowacka,<sup>2</sup> Ineke Neefs,<sup>1</sup> Josef Ecker,<sup>3</sup> Marcus Höring,<sup>4</sup> Gerhard Liebisch,<sup>4</sup> Cathy Debier,<sup>1</sup> Olivier Feron,<sup>2</sup> and Yvan Larondelle<sup>1,5,\*</sup>

## SUMMARY

**Ferroptosis is a cell death pathway that can be promoted by peroxidizable polyunsaturated fatty acids in cancer cells. Here, we investigated the mechanisms underlying the toxicity of puniceic acid (PunA), an isomer of conjugated linolenic acids (CLnAs) bearing three conjugated double bonds highly prone to peroxidation, on prostate cancer (PCa) cells. PunA induced ferroptosis in PCa cells and triggered massive liposome remodeling, more strongly in PC3 androgen-negative cells than in androgen-positive cells. The greater sensitivity of androgen-negative cells to PunA was associated with lower expression of glutathione peroxidase 4 (GPX4). We then identified the phospholipase PLA2G7 as a PunA-induced ferroptosis suppressor in PCa cells. Overexpressing PLA2G7 decreased lipid peroxidation levels, suggesting that PLA2G7 hydrolyzes hydroperoxide-containing phospholipids, thus preventing ferroptosis. Importantly, overexpressing both PLA2G7 and GPX4 strongly prevented PunA-induced ferroptosis in androgen-negative PCa cells. This study shows that PLA2G7 acts complementary to GPX4 to protect PCa cells from CLnA-induced ferroptosis.**

## INTRODUCTION

Ferroptosis is an iron-reliant cell death pathway that is triggered by the overwhelming accumulation of lipid hydroperoxides generated from the oxidation of polyunsaturated fatty acids (PUFAs).<sup>1,2</sup> Lipid hydroperoxides and their derived lethal breakdown molecules may accumulate to an extent that outperforms cell antioxidant capacities, leading to cell membrane rupture and ferroptosis.<sup>1–5</sup> Among cell antioxidant repair systems, glutathione peroxidase 4 (GPX4) has been shown to have a major anti-ferroptotic impact by reducing lipid hydroperoxides into harmless alcohols using glutathione.<sup>6</sup> The cystine-glutamate antiporter XCT supports GPX4 activity by importing cystine, a major precursor in glutathione synthesis.<sup>1</sup> Other ferroptosis suppressors have been discovered, such as ferroptosis suppressive protein (FSP1)<sup>7,8</sup> and dihydrofolate reductase (DHFR),<sup>9</sup> which regenerate the endogenous antioxidants coenzyme Q10<sup>7,8</sup> and tetrahydropterin BH4,<sup>9</sup> respectively. On the contrary, the uptake and intracellular accumulation of PUFAs promote ferroptosis, through their activation in their acyl-CoA form by the action of acyl-CoA synthetase 4 (ACSL4),<sup>10,11</sup> preferentially favoring their subsequent incorporation within prone-to-peroxidation phospholipid species.<sup>10,12</sup> Cell sensitivity to ferroptosis thus depends on how cells manage the balance between their cellular antioxidant capacities and their pool of peroxidizable PUFAs.

Since ferroptosis was brought to light in 2012,<sup>1</sup> the interest for inducing ferroptosis to eliminate cancer cells, particularly therapy-resistant cells, has been growing.<sup>13–16</sup> Multiple pro-ferroptotic drugs have been identified, especially GPX4 inhibitors such as Ras-selective lethal molecule (RSL3).<sup>17</sup> On the other hand, many studies have highlighted the potential of supplementing cancer cells with PUFAs as lipid peroxidation substrates to promote ferroptosis.<sup>12,18</sup> Among PUFAs, conjugated linolenic acids (CLnAs) have proven to be particularly interesting PUFAs as they are capable of inducing ferroptosis in cancer cells as single agents.<sup>19–21</sup> Plant-derived CLnAs are positional and geometrical isomers of  $\alpha$ -linolenic acid with three conjugated double bonds, which makes them 2.5 times more susceptible to autoxidation than their non-conjugated counterpart, due to the fast electron delocalization at the conjugated double bonds.<sup>22,23</sup> Moreover, it has been recently shown that CLnAs have distinct mechanisms of peroxidation compared with *bona fide* PUFAs, leading to the greater generation of deleterious electrophilic aldehydes and further contributing to their pro-ferroptotic potential.<sup>20</sup> CLnAs therefore offer a new therapeutic strategy to promote ferroptosis in cancer cells.

<sup>1</sup>Louvain Institute of Biomolecular Science and Technology, UCLouvain, 1348 Louvain-la-Neuve, Belgium

<sup>2</sup>FATH, Institut de recherche Expérimentale et Clinique, UCLouvain, 1200 Woluwe Saint-Lambert, Belgium

<sup>3</sup>Functional Lipidomics and Metabolism Research, Institute of Clinical Chemistry and Laboratory Medicine, University Hospital Regensburg, Regensburg, Germany

<sup>4</sup>Lipidomics Lab, Institute of Clinical Chemistry and Laboratory Medicine, University Hospital of Regensburg, Regensburg, Germany

<sup>5</sup>Lead contact

\*Correspondence: [yvan.larondelle@uclouvain.be](mailto:yvan.larondelle@uclouvain.be)

<https://doi.org/10.1016/j.isci.2024.109774>



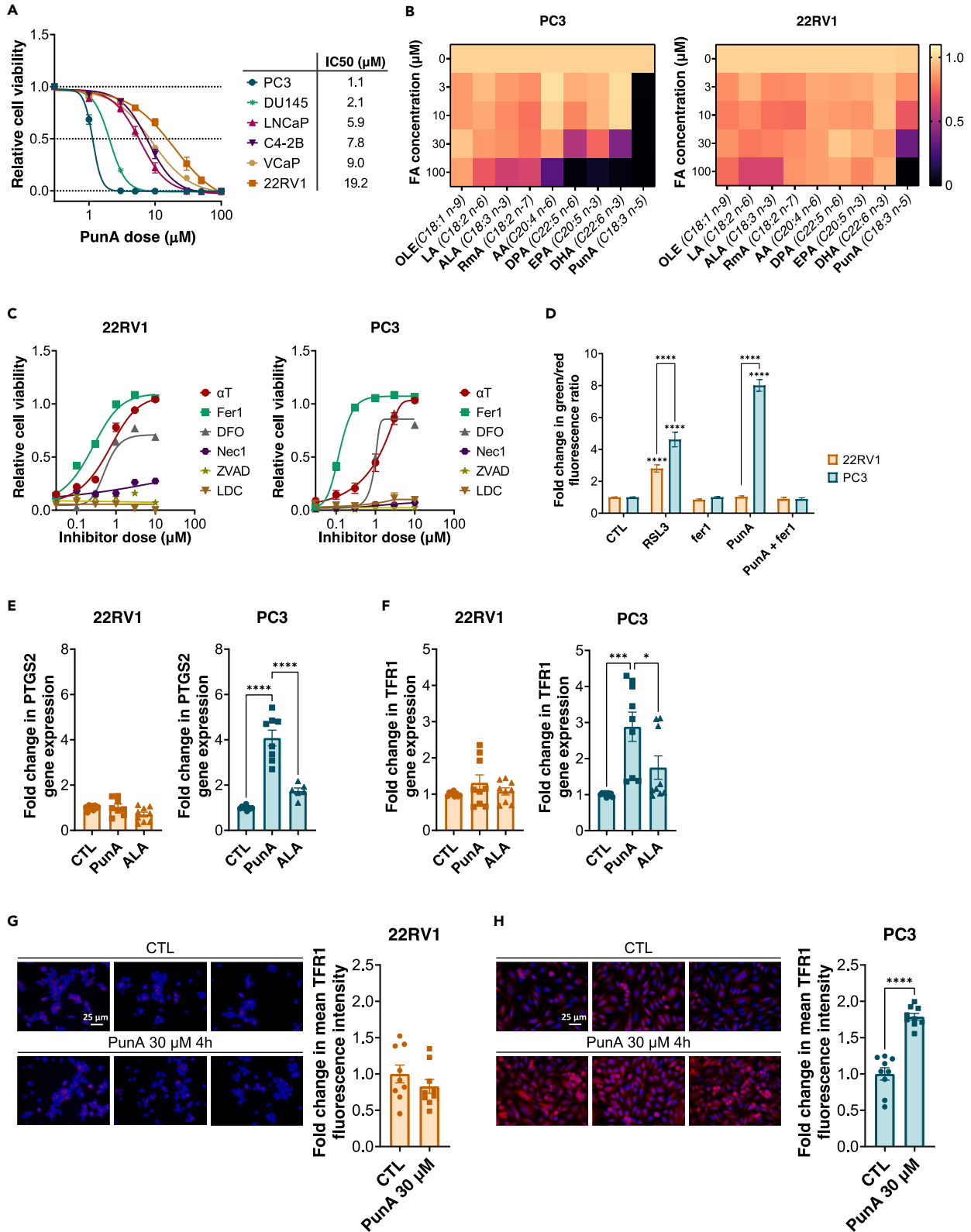


**Figure 1. Punicic acid induces ferroptosis in PCa cells**

(A) Relative viability of PC3, DU145, LNCaP, C4-2B, VCaP, and 22RV1 cells after 72 h of puniolic acid (PunA) treatment at increasing doses, normalized to the control (untreated cells). Associated IC50 values are found in the table on the right.

(B) Relative viability of PC3 and 22RV1 cells after 72 h of treatment with monounsaturated FAs (oleic acid, OLE) or polyunsaturated FAs (LA, linoleic acid; ALA,  $\alpha$ -linolenic acid; RmA, rumenic acid; AA, *n*-6 arachidonic acid; DPA, *n*-6 docosapentaenoic acid; EPA, *n*-3 eicosapentaenoic acid; DHA, *n*-3 docosahexaenoic acid; PunA, puniolic acid), normalized to the control (untreated cells). See [Table S3](#) for the detailed FA structures.

(C) Relative viability of PC3 and 22RV1 cells after 72 h of PunA treatment (i.e., 3 and 30  $\mu$ M for PC3 and 22RV1 cells, respectively, selected on the basis of the established dose-response curves to sufficiently deplete cell viability) with increasing doses of  $\alpha$ -tocopherol ( $\alpha$ T), ferrostatin-1 (fer1), deferoxamine mesylate (DFO), necrostatin-1 (Nec1), Z-VAD-fmk (ZVAD), or LDC7559 (LDC), normalized to the control (DMSO 0.1%v/v).

(D) Lipid peroxidation levels in PC3 and 22RV1 cells after 4 h of treatment with Ras-selective lethal 3 (RSL3) 1  $\mu$ M, fer1 10  $\mu$ M, PunA 30  $\mu$ M, or a combination of PunA 30  $\mu$ M and fer1 10  $\mu$ M. Data are expressed as the fold change in the green-to-red fluorescence ratio of C11-BODIPY, normalized to the control (untreated cells).

(E and F) Fold change in gene expression of prostaglandin-endoperoxide synthase 2 (PTGS2) (E) and transferrin receptor 1 (TFR1) (F) in 22RV1 and PC3 cells treated for 24 h with PunA or ALA 1.5  $\mu$ M, normalized to the control (untreated cells). The dose was selected on the basis of the established dose-response curves (A), so that PC3 cells were still viable at 24 h of treatment. Data points represent individual RT-qPCR technical replicates ( $N = 3$ ,  $n = 3$ ).

(G and H) Fold change in TFR1 relative fluorescence intensity in 22RV1 and PC3 cells treated for 4 h with PunA 30  $\mu$ M, normalized to DAPI fluorescence intensity and the control (untreated cells). Representative pictures of TFR1 fluorescence in 22RV1 and PC3 cells are shown (scale bars, 25  $\mu$ m). Data of (A) and (C) were fitted with dose-response curves. (B) The doses at which the drop in PC3 cell viability was determined to be significant by two-way ANOVA were 3  $\mu$ M for PunA, 30  $\mu$ M for DPA and DHA, and 100  $\mu$ M for LA, ALA, RmA, AA, and EPA. The dose at which the drop in 22RV1 cell viability was determined to be significant was 30  $\mu$ M for PunA, only, all other FAs leading to no significant losses in cell viability. Data are represented as mean  $\pm$  SEM of  $N \geq$  three independent cultures (A, C–F) or of nine independent pictures (G–H). Significance was established by one-way ANOVA with Sidak's multiple comparisons (A–C, E, F), by two-way ANOVA with Sidak's multiple comparison (D) or by Student's *t* test (G, H). \* $p < 0.05$ , \*\* $p < 0.01$ , \*\*\* $p < 0.001$ , \*\*\*\* $p < 0.0001$ . See also [Figure S1](#) and [Table S3](#).

Prostate cancer (PCa) is the second most leading cancer among men worldwide.<sup>24</sup> To survive and thrive, PCa cells need to alter their metabolism. However, instead of increasing their glycolytic rates as most cancer cells, PCa cells preferentially develop an increased lipid metabolism to sustain cell proliferation and meet biosynthetic needs.<sup>25,26</sup> Features of PCa cell metabolism dysregulation include enhanced *de novo* fatty acid (FA) synthesis, high extracellular FA uptake, strong triglyceride (TG) accumulation in lipid droplets, and increased FA  $\beta$ -oxidation.<sup>26–28</sup> Interestingly, this dependence on FA metabolism is associated with disease progression and the development of hormone therapy resistance.<sup>28</sup> Such an addiction to extracellular FA uptake makes PCa a particularly attractive cancer type for the promotion of ferroptosis. Yet, few studies have focused on the induction of ferroptosis in PCa. For instance, it has been shown that androgen deprivation leads to an increase in the unsaturation level of membrane phospholipids and greater lipid peroxidation, resulting in hypersensitivity to ferroptosis.<sup>29</sup> Another study demonstrated that blocking PUFA  $\beta$ -oxidation in PCa cells leads to their accumulation and enhanced sensitivity to ferroptosis inducers.<sup>30</sup> Nevertheless, the potential of inducing ferroptosis by using the reliance of PCa cells on extracellular FAs as a lure has never been investigated, and the drivers of PCa cell sensitivity to ferroptosis remain largely unexplored, if not unknown in the context of CLnA-induced ferroptosis.

In the present study, we investigated the mechanisms determining the sensitivity of PCa cells to CLnA-induced ferroptosis. We show that puniolic acid (PunA), a CLnA isomer, induces ferroptosis in PCa cells, but more powerfully in androgen-negative cells than in androgen-positive cells. PunA triggers a massive remodeling of cellular lipidome, especially in PC3 androgen-negative cells. Although the difference in PunA sensitivity between PCa cells correlates with GPX4 and ACSL4 expression, we show that altering ACSL4 or GPX4 expression only partially changes PCa cell sensitivity to PunA. We then demonstrate that the phospholipase PLA2G7 plays a role in the suppression of CLnA-induced ferroptosis in PCa cells. Overexpression of PLA2G7 in PC3 cells decreases lipid peroxidation levels, suggesting that PLA2G7 hydrolyzes hydroperoxide-containing phospholipids (PLs), removing them from cell membranes and preventing ferroptosis. More importantly, blockade of both PLA2G7 and GPX4 strongly increases lipid peroxidation and PunA sensitivity in androgen-positive cells. Our results show that the phospholipase PLA2G7 acts complementary to GPX4 to eliminate lipid hydroperoxides from cell membranes and thus protects PCa cells from CLnA-induced ferroptosis.

## RESULTS

### Puniolic acid induces ferroptosis in PCa cells

The effect of PunA was assessed in six PCa cell lines with diverse androgenic backgrounds (i.e., androgen-positive sensitive LNCaP and VCaP, androgen-positive insensitive 22RV1 and C4-2B, and androgen-independent PC3 and DU145 cells). PunA was cytotoxic to all PCa cells ([Figure 1A](#)). Surprisingly, however, PC3 and DU145 androgen-negative cells appeared significantly more sensitive to PunA toxicity than LNCaP, C4-2B, and VCaP cells, themselves being more sensitive than 22RV1 cells, with IC50 values of 1.1, 2.1, 5.9, 7.8, 9.0, and 19.2  $\mu$ M, respectively ([Figure 1A](#)). We then compared the effect of PunA with that of other FAs with different chain lengths and degrees of unsaturation ([Table S3](#)) in PC3, LNCaP, and 22RV1 cells. The cytotoxicity of FAs on PC3 cells increased with the degree of unsaturation and chain length ([Figure 1B](#)). However, the effect of non-conjugated PUFAs on PC3 cells was only observed at a dose 10 times higher than that of PunA in the case of DPA and DHA (i.e., 30  $\mu$ M), or even higher for the other PUFAs (i.e., 100  $\mu$ M) ([Figure 1B](#)), emphasizing the stronger effect of PunA compared with the non-conjugated PUFAs. Moreover, none of the non-conjugated FAs tested was significantly cytotoxic to 22RV1 cells, and only PunA significantly decreased cell viability ([Figure 1B](#)). Similar trends were observed for the LNCaP cell line ([Figure S1A](#)). These results confirm that PunA is cytotoxic to PCa cells, although the different cell lines show significant differences in their PunA sensitivity.

We next aimed to evaluate whether PunA induces ferroptotic cell death in PCa cells, using both a highly sensitive cell line (PC3) and a more resistant cell line (22RV1). We first measured cell viability upon treatment with a cell-line specific lethal dose of PunA and an increasing dose of a ferroptosis inhibitor. Both  $\alpha$ -tocopherol and ferrostatin-1 (fer1), which are two ferroptosis inhibitors with radical trapping antioxidant activity, completely restored cell viability in both PC3 and 22RV1 cells (Figure 1C). Deferoxamine mesylate, an iron chelator, also inhibited the effect of PunA in both cell lines, but to a lesser extent (Figure 1C). In contrast, ammonium tetrathiomolybdate, a copper chelator preventing cupropitosis,<sup>31</sup> did not significantly inhibit the toxicity of PunA on both PC3 and 22RV1 cells (Figure S1B). In addition, neither the apoptosis inhibitor ZVAD-fmk, the necroptosis inhibitor necrostatin-1 nor the pyroptosis inhibitor LDC7559 significantly inhibited the effect of PunA (Figure 1C), showing that PunA specifically induces ferroptosis in PCa cells. To further confirm that PunA triggers ferroptosis, we measured changes in lipid peroxidation levels in PCa cells after PunA treatment for 4 h. PunA significantly increased lipid peroxidation levels by 8-fold in PC3 cells compared with control, but not in 22RV1 cells (Figure 1D), further highlighting the difference in sensitivity between PCa cell lines. This rise in lipid peroxidation was fully inhibited by the addition of fer1 (Figure 1D). Interestingly, upon treatment with the classical ferroptosis inducer and GPX4 inhibitor RSL3, the level of lipid peroxidation increased in both cell lines, by 5- and 3-fold in PC3 and 22RV1 cells, respectively (Figure 1D), coinciding with the loss of cell viability observed in both cell lines upon RSL3 treatment (Figure S1C). Importantly, the difference in cell line sensitivity between PC3 and 22RV1 cells was significantly higher for PunA than for RSL3, suggesting potentially distinct mechanisms of ferroptosis induction between the two compounds. Finally, we examined the changes in gene expression for two ferroptosis markers, prostaglandin synthetase PTGS2<sup>32</sup> and transferrin receptor TFR1.<sup>33</sup> PunA significantly increased gene expression of both PTGS2 and TFR1 compared with control in PC3 cells but not in 22RV1 cells for the same dose (Figures 1E and 1F). On the contrary,  $\alpha$ -linolenic acid (ALA), the non-conjugated counterpart of PunA, did not alter PTGS2 and TFR1 gene expression (Figures 1E and 1F), further demonstrating the stronger ability of CLnAs to induce ferroptosis. Moreover, TFR1 protein abundance was also significantly increased upon acute treatment with PunA 30  $\mu$ M for 4 h in PC3 cells but not in 22RV1 cells (Figures 1G and 1H). These results confirm that PunA induces ferroptosis in PCa cells but also highlight significant differences in PunA sensitivity between PCa cell lines.

### Punic acid triggers a deep remodeling of the intracellular lipidome in PCa cells

We hypothesized that PunA induces ferroptosis by being taken up and incorporated into specific intracellular lipids, where it can then be peroxidized. We first treated PCa cells with PunA 30  $\mu$ M for 2, 4, 6 or 8 h and measured PunA cellular uptake and incorporation by analyzing the FA content of PCa cells in three intracellular fractions: neutral lipids (NLs, mainly composed of TGs), free fatty acids (FFAs), and phospholipids (PLs). PunA was taken up and incorporated into all three fractions in both PC3 and 22RV1 cells (Figure 2A). PunA was distributed between NLs, FFAs, and PLs at 39%–49%, 1%, and 50%–60% of its total intracellular amount, respectively, after 4 h of treatment, with no significant differences between cell lines (Figure 2A). Enrichment of NL and PL in PunA (i.e., amount of PunA normalized to the total amount of FAs in each fraction, in moles) increased over time in both 22RV1 and PC3 cells to around 20% (n/n) of the FAs in NLs and 10% (n/n) of the FAs in PLs (Figure 2B). This enrichment was not associated to an overall increase in the total amount of FAs in NLs and PLs over time in both cell lines (Figure S2A), suggesting that the enrichment is due to the preferential accumulation of PunA, which replaces other acyl chains. More importantly, PunA was incorporated significantly faster and in greater amounts in the NLs of PC3 cells compared with 22RV1 cells at 2 and 4 h of treatment (Figure 2B). Surprisingly, no such difference between 22RV1 and PC3 cells was seen for the PL fraction (Figure 2B). Interestingly, after PunA treatment for 4 h, the ratio of PUFAs to monounsaturated FAs (MUFAs) in the NL fraction increased significantly in both 22RV1 and PC3 cells compared with control conditions, but was significantly higher in PC3 cells than in 22RV1 cells (Figure 2C). As for the PL fraction, the PUFAs-to-MUFAs ratio increased after PunA treatment for PC3 cells, but not for 22RV1 cells (Figure 2D). This increase was associated with both a drop in total MUFA amount and especially a rise in total PUFA amount in both NL and PL fractions (Figure S2B). These results also suggest that PC3 cells may be intrinsically more sensitive to ferroptosis because of a greater propensity to accumulate PUFAs.

We further investigated the changes that occur in the lipidome of PCa cells under the effect of PunA. We performed a lipidomic analysis of PCa cells treated with either control, PunA 2.5 to 10  $\mu$ M, ALA 10  $\mu$ M, fer1 10  $\mu$ M, or a combination of PunA 10  $\mu$ M and fer1 10  $\mu$ M. Principal component analysis revealed that the lipidome and the changes of lipidome that occur with the different treatments are sufficient to distinguish PC3, 22RV1, and LNCaP cell lines from each other (Figure 3A), highlighting significant differences in lipid composition and response of PCa cells to the different treatments. Using regression and differential expression analysis, we identified the lipid species whose abundance changed when PCa cells were treated with PunA 10  $\mu$ M compared with the control. Overall, PunA induced a massive remodeling of the intracellular lipidome in all three PCa cell lines (Figures 3B–3D), with more significant changes in PC3 cells (Figure 3B). Indeed, the number of altered lipid species and the magnitude of changes in lipid species abundance were significantly higher in PC3 cells than in the two other cell lines (Figures 3B–3D). Specifically, PunA induced a rise in the amount of various TG species (e.g., TG 48:3, TG 52:5, and TG 50:3, among others), again with greater changes observed in PC3 cells (Figures 3B–3D). In fact, PunA triggered a significant increase of the total amount of TG species with more than 3 double bonds in PC3 and LNCaP cells but not in 22RV1 cells (Figure S3A). Of note, we also observed a rise in the concentration of the cholesteryl ester CE 18:3, probably corresponding to a PunA acyl chain, in PC3 and LNCaP cells (Figures 3B–3D). These results confirm the incorporation of PunA into intracellular NLs. In addition, PunA induced a significant increase in the abundance of phosphatidylcholine (PC) and phosphatidylethanolamine (PE) species (Figures 3B–3D), in particular of PC 34:3, PC 34:4, PC 36:6, and PE 34:3, suggesting an incorporation of PunA in these PL species. The increase in the amounts of these PC and PE species was PunA dose-dependent in the three cell lines and was also observed upon treatment with ALA, except for PC 36:6 in LNCaP cells and PE 34:3 for both 22RV1 and LNCaP cells (Figure S3B), suggesting that these changes are not specific to conjugated PUFAs. Surprisingly, no changes in the abundance of ether-PL species was observed, suggesting that PunA does not incorporate in ether lipids in PCa cells (Figures 3B–3D). Importantly, PC3 cells, but not

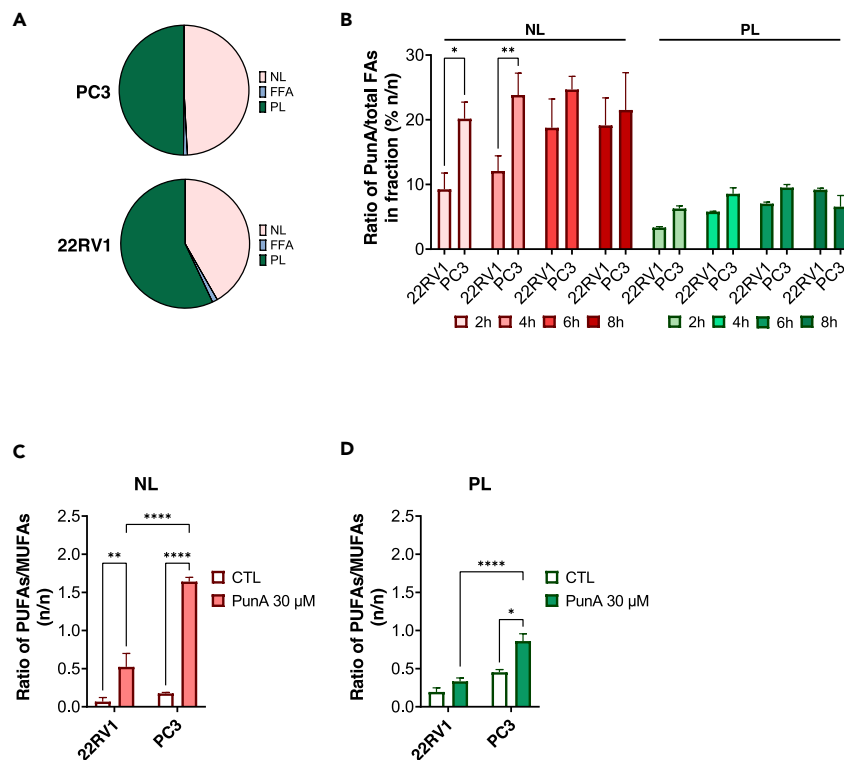


**Figure 2. Punicic acid is incorporated in both neutral lipids and phospholipids of Pca cells**

(A) Distribution of punicic acid (PunA) between neutral lipids (NL), free fatty acids (FFA), and phospholipids (PL) of PC3 and 22RV1 cells treated with PunA 30 μM for 4 h. Data are expressed as the ratio of the amount of PunA in a given fraction to the total amount of PunA in the cells, in % (n/n).

(B) Enrichment in PunA in NL and PL of 22RV1 and PC3 cells treated with PunA 30 μM for 2, 4, 6, or 8 h. Data are expressed as the ratio of the amount of PunA to the amount of all FAs in a given fraction, in % (n/n).

(C and D) Ratios of polyunsaturated FAs (PUFAs)-to-monounsaturated FAs (MUFAs) in (C) the NL or (D) the PL fraction of 22RV1 and PC3 cells either untreated (control) or treated with PunA 30 μM for 4 h. Data are represented as mean ± SEM of N = 3 independent cultures (B–D). Significance was established by two-way ANOVA with Sidak's multiple comparisons (B–D). \*p < 0.05, \*\*p < 0.01, \*\*\*p < 0.001, \*\*\*\*p < 0.0001. See also Figure S2.

22RV1 and LNCaP cells, were faced with a significant rise in the abundance of PE 36:6 when treated with the highest dose of PunA but not with ALA (Figure 3E). PE 36:6 may be composed of two PunA acyl chains. As the double bonds of PunA follow a *cis-trans-cis* configuration, the acyl chain is more linear than the *cis-cis-cis* configuration of ALA (Table S3), which would explain why the abundance of PE 36:6 only increases significantly with PunA. Taken together, our results show that PunA is incorporated in various intracellular lipids, particularly into PL species, in a way that strongly correlates with cell line sensitivity to PunA.

### Sensitivity to punicic-acid-induced ferroptosis partly depends on GPX4 and ACSL4 in PCa cells

In order to examine the mechanisms behind the difference in the sensitivity of PCa cell lines to PunA, we first looked at the expression of ACSL4, a protein that is involved in ferroptosis through PUFA activation and incorporation within PLs.<sup>10</sup> For this purpose, we used the two cell lines showing the greatest difference in PunA sensitivity (i.e., PC3 and 22RV1 cells). PC3 cells expressed significantly more ACSL4 than 22RV1 cells, at both mRNA (Figure 4A) and protein (Figure 4B) levels. ACSL4 protein abundance was not altered by the addition of PunA nor ALA in either cell line (Figure 4B). To further investigate the role of ACSL4 in PunA toxicity and cell line sensitivity, we inhibited ACSL4 by using rosiglitazone (Rosi), a peroxisome proliferator-activated receptor γ agonist with proven anti-ACSL4 activity.<sup>34,35</sup> Although the addition of Rosi did not alter the effect of PunA on ACSL4<sup>low</sup> 22RV1 cell viability, it partially restored the viability of ACSL4<sup>high</sup> PC3 cells treated with a lethal dose of PunA (Figure 4C). More importantly, knockdown of ACSL4 significantly inhibited PunA toxicity (Figures 4D and 4E) and reduced the increase in PunA-induced lipid peroxidation in PC3 cells (Figure 4F), which were both completely abolished when fer1 was added. ACSL4 knockdown in PC3 cells also decreased the amount of PunA in both PLs and NLs compared with control cells, whereas it increased the amount of PunA in its FFA form (Figure 4G). Of note, inhibition of diacylglycerol acyl transferase DGAT1, an enzyme catalyzing the last step of TG synthesis, decreased the amount of PunA in the NL fraction of both 22RV1 and PC3 cells and increased PunA toxicity (Figures S4A and S4B). Altogether, these data indicate that PunA toxicity derives from its ACSL4-dependent incorporation in the PL fraction and not into TGs, as previously suggested.<sup>21</sup>

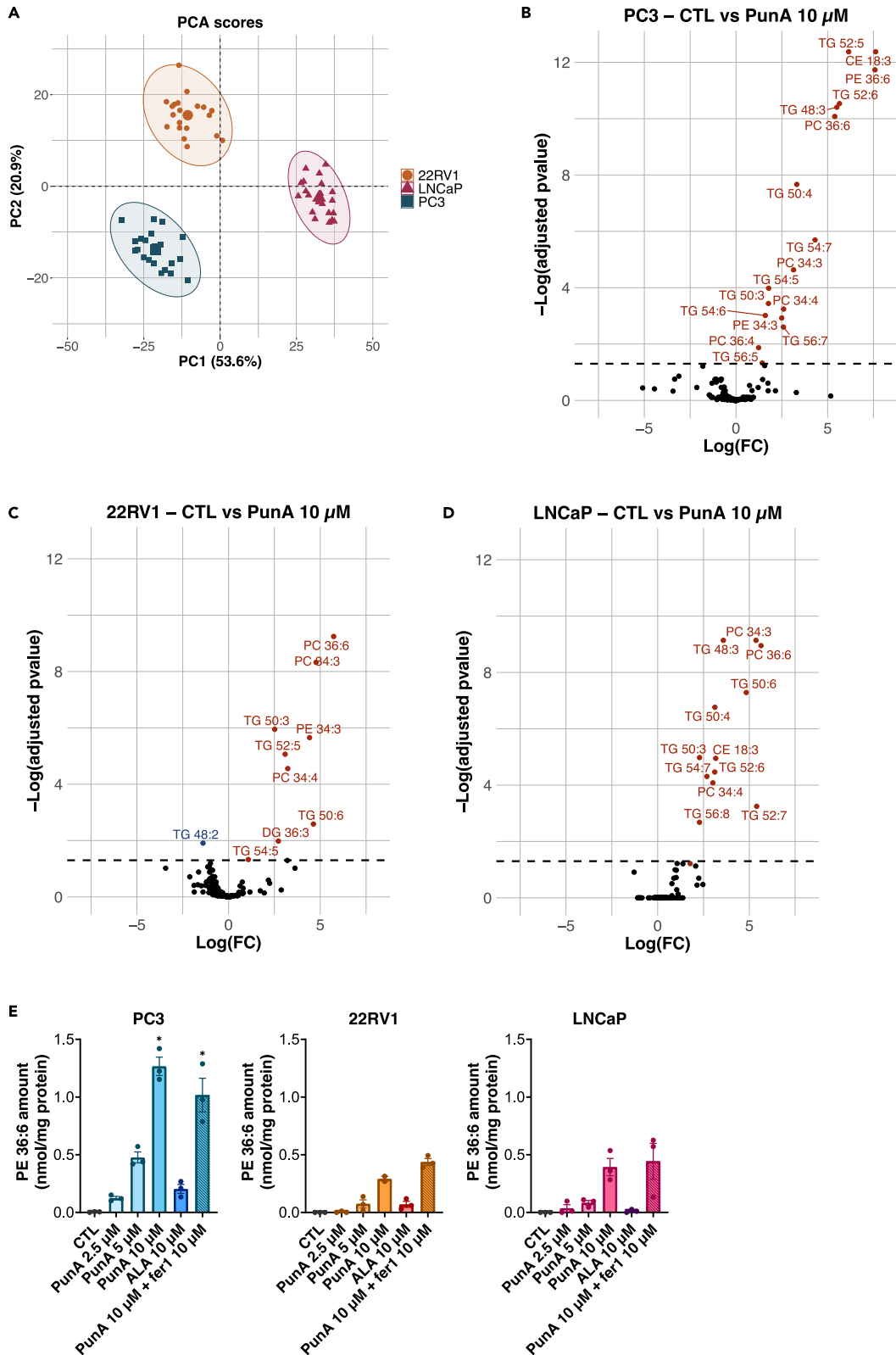


**Figure 3. Punicic acid triggers a deep remodeling of the intracellular lipidome in Pca cells**

(A) Scores plot from principal-component analysis (PCA) for the two first dimensions on the three cell lines (i.e., PC3, 22RV1, and LNCaP), for all lipid species and all treatments. Each dot represents one replicate for one treatment, and the larger dot represents the center of each ellipse for each cell line. (B–D) Volcano plots of significance ( $-\log_2$  of adjusted  $p$  value) and  $\log_2$  fold change in lipid species abundance for (B) PC3, (C) 22RV1, and (D) LNCaP cells treated for 4 h with puniceic acid (PunA) 10  $\mu\text{M}$  compared with control (untreated cells). Species whose abundance increased or decreased with the treatment are shown in red or blue, respectively. (E) Abundance of the phosphatidylethanolamine (PE) 36:6 species in PC3, 22RV1, and LNCaP cells after 4 h of treatment with control (no treatment); PunA 2.5, 5, or 10  $\mu\text{M}$ ,  $\alpha$ -linolenic acid (ALA) 10  $\mu\text{M}$ ; or a combination of PunA 10  $\mu\text{M}$  and ferrostatin-1 (fer1) 10  $\mu\text{M}$ . Data are represented as mean  $\pm$  SEM of  $N = 3$  independent cultures (E). Significance was established by false-discovery rate with Benjamini-Hochberg  $p$  value adjustment for multiple comparisons (B–E). \*corresponds to positive discovery. See also Figure S3.

We next explored the role of GPX4, a major ferroptosis suppressor, in PunA toxicity and differential cell line sensitivity. PC3 cells expressed significantly less GPX4 than 22RV1 cells, both at mRNA (Figure 5A) and protein (Figure 5B) levels. The expression of GPX4 was not altered by PunA or ALA in either cell line (Figure 5B). Cotreatment with sublethal doses of PunA and the well-known GPX4 inhibitor RSL3 significantly increased PunA toxicity in 22RV1 and PC3 cells (Figure 5C), suggesting that GPX4 may indeed help preventing PunA toxicity. More importantly, GPX4 knockdown in 22RV1 cells strongly increased the effect of PunA on cell viability (Figures 5D and 5E), which was accompanied by a sharp rise in the level of lipid peroxidation, as compared with native 22RV1 cells (Figure 5F). These effects on cell viability and lipid peroxidation were completely inhibited by the addition of fer1 (Figures 5E and 5F). Furthermore, overexpression of GPX4 in PC3 cells resulted in a weak but significant inhibition of PunA toxicity, as well as of that of RSL3 at low doses (Figures 5G and 5H). These results highlight the essential role of GPX4 in 22RV1 cells to counteract PunA-induced ferroptosis. GPX4 re-expression in PC3 cells, however, appears not to be sufficient to completely prevent PunA-induced ferroptosis, suggesting that other enzymes may be involved.

The analysis of the expression of other genes known to be involved in ferroptosis yielded rather inconsistent results. DHFR was significantly more expressed in 22RV1 cells than in PC3 cells at the protein level but not at the mRNA level (Figures S5A and S5B). XCT was significantly more expressed by PC3 cells than 22RV1 cells at the mRNA level, but this difference between cell lines was not confirmed at the protein level (Figures S5C and S5D). Similar trends were observed for FSP1 (Figures S5E and S5F). As FSP1 is a major ferroptosis suppressor, we investigated its role in the protection of PC3 cells against PunA toxicity, especially considering that GPX4 seems to play a rather minor role in this cell line. The addition of iFSP1, a specific FSP1 inhibitor, induced a marginal decrease in PC3 cell viability, as compared with the addition of different GPX4 inhibitors (i.e., the XCT inhibitor imidazole ketone erastin [IKE], ML210 and RSL3, which directly inhibit GPX4) (Figure S5G). Unexpectedly, the addition of PunA did not significantly enhance the effect of iFSP1, nor of the different GPX4 inhibitors (Figure S5G). Moreover, the addition of CoQ10, the endogenous antioxidant regenerated by FSP1, did not inhibit PunA toxicity on PC3 cells (Figure S5H). These results suggest that FSP1 is not able to prevent PunA-induced ferroptosis in PCa cells with low GPX4 levels.

**Phospholipase PLA2G7 is involved in the suppression of puniceic-acid-induced ferroptosis in Pca cells**

Our lipidomic results suggest that PunA incorporation into specific PL species may account for PunA toxicity and, at least in part, for the difference in sensitivity between PCa cell lines. We therefore explored databases to identify key enzymes that might be involved in PunA toxicity and could explain the greater sensitivity of PC3 cells compared with 22RV1 cells. We crossed the Cancer Cell Line Encyclopedia gene expression dataset ([www.depmap.org](http://www.depmap.org)) with a list of genes involved in FA metabolism and PL remodeling compiled from the Gene Set Enrichment Signature datasets ([www.gsea-msigdb.org](http://www.gsea-msigdb.org)). This enabled us to identify six genes differentially expressed between 22RV1 and PC3 cells (Figure 6A): ACSL6, PAFAH1B3, PLA2G10, PLA2G4E, PLA2G6, and PLA2G7. Among these genes, three stand out as being particularly involved in the remodeling of PC and PE acyl chains: PLA2G10, PLA2G6, and PLA2G7. Group X phospholipase PLA2G10 is involved in the transfer of PUFAs from membrane PLs to lipid droplets to support lipid mediator production.<sup>36</sup> Group VI and VII phospholipases PLA2G6 and PLA2G7 are capable of hydrolyzing membrane PLs carrying peroxidized fatty acyl chains,<sup>37–40</sup> although only PLA2G6 has been reported in the context of ferroptosis. We confirmed that PLA2G10, PLA2G6, and PLA2G7 are significantly more expressed in 22RV1 cells than in PC3 cells at the mRNA level (Figure 6B). To identify whether any of these three candidates would have a clinical relevance, we screened for their expression in tissues from PCa patients from the TCGA cohort. Importantly, PLA2G7 was significantly more expressed in PCa tissues than in normal prostate tissues ( $p$  value of  $1.6 \times 10^{-11}$ ) (Figure 6C), emphasizing its clinical relevance in the context of PCa.

We further investigated the potential relationship between PLA2G7 expression and the sensitivity of PCa cell lines to PunA-induced ferroptosis. Interestingly, PunA increased PLA2G7 mRNA expression relative to control in 22RV1 cells, whereas it decreased PLA2G7 expression in PC3 cells (Figure 6D). In contrast, PunA did not influence PLA2G6 and PLA2G10 gene expression (Figures S6A and S6B). As for protein abundance, PLA2G7 levels were significantly higher in 22RV1 cells than in PC3 cells but were not influenced by PunA or ALA treatment (Figure 6E). We next used Darapladib, a PLA2G7-specific inhibitor. Darapladib significantly increased PunA toxicity in 22RV1 cells (Figure 6F). Furthermore, PunA treatment marginally decreased 22RV1 cell viability when PLA2G7 was knocked down, although a high dose of PunA was required (Figures 6G, 6H, and S6C). Conversely, PLA2G7 overexpression in PC3 cells significantly reduced the effect of PunA on cell viability (Figures 6I, 6J, and S6D) and reduced the PunA-induced increase in lipid peroxidation (Figure 6K), although not to the level of the control conditions. Interestingly, PLA2G7 overexpression did not change the sensitivity of PC3 cells to RSL3 (Figures S6E and S6F), suggesting that PunA and classical ferroptotic drugs may induce ferroptosis through different mechanisms. We also tested the impact of the ferroptosis suppressor PLA2G6 on PunA toxicity. However, although PLA2G6 inhibition with a specific inhibitor (i.e., FKGI18) increased PunA toxicity in 22RV1 cells (Figure S6G), PLA2G6 knockdown in 22RV1 cells did not influence PunA toxicity as did PLA2G7 knockdown (Figures S6H–S6J),

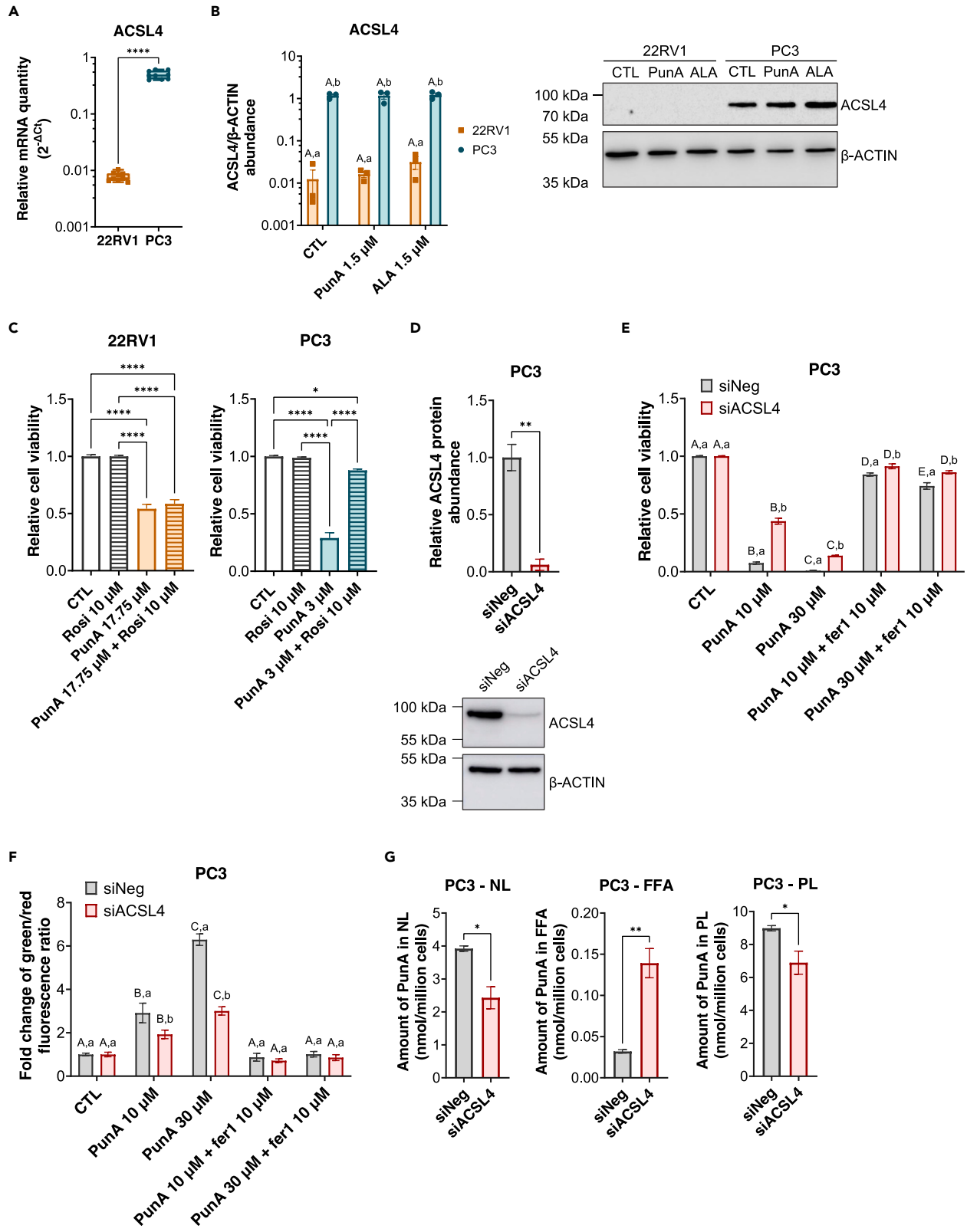


**Figure 4. Sensitivity to puni-c-acid-induced ferroptosis partly depends on its ACSL4-driven incorporation into phospholipids in PCa cells**

(A) Relative mRNA quantity of ACSL4 in 22RV1 and PC3 cells, expressed as  $2^{-\Delta C_t}$  with the geometric mean of the Ct of three reference genes (i.e., GUSB, TBP, and  $\beta$ -ACTIN). Data points represent individual RT-qPCR technical replicates ( $N = 3$ ,  $n = 3$ ).

(B) Ratio of ACSL4-to- $\beta$ -ACTIN protein abundance in 22RV1 and PC3 cells treated with either no fatty acid (FA) (control), puni-c acid (PunA) 1.5  $\mu$ M, or  $\alpha$ -linolenic acid (ALA) 1.5  $\mu$ M for 24 h. Representative western blot is shown on the right.

(C) Relative viability of 22RV1 and PC3 cells after treatment with either vehicle (DMSO 0.1% v/v, control), rosiglitazone 10  $\mu$ M (Rosi), PunA 17.75 or 3  $\mu$ M, respectively, or a combination thereof, for 24 h, normalized to the control. The doses of PunA were selected on the basis of the dose-response curves established in [Figure 1A](#), to significantly deplete cell viability in both cell lines at 24 h.

(D) Relative ACSL4 protein abundance in PC3 cells transfected with either a negative control siRNA (siNeg) or a siRNA pool targeting ACSL4 (siACSL4), normalized to  $\beta$ -ACTIN protein abundance and to siNeg. Representative western blot is shown below.

(E) Relative viability of siNeg and siACSL4 PC3 cells treated with either PunA, ferrostatin-1 (fer1), or a combination thereof for 24 h, normalized to the control (untreated cells).

(F) Lipid peroxidation levels of siNeg and siACSL4 PC3 cells treated with PunA, fer1, or a combination thereof, at the indicated doses, for 4 h. Data are expressed as the fold change in the green-to-red fluorescence ratio of C11-BODIPY and normalized to control (untreated cells).

(G) Amount of PunA in neutral lipids (NL), free FA (FFA), or phospholipids (PL) of siNeg and siACSL4 PC3 cells treated with PunA 30  $\mu$ M for 4 h. Data were normalized to the number of cells (in millions). Data are represented as mean  $\pm$  SEM of  $N \geq 3$  independent cultures (B–G) or as median with the 25–75 percentiles of nine replicates (A). Significance was established by Student's t test (A,D,G), one-way ANOVA with Sidak's multiple comparisons (C), or two-way ANOVA with Sidak's multiple comparisons (B, E, F). \* $p < 0.05$ , \*\* $p < 0.01$ , \*\*\* $p < 0.001$ , \*\*\*\* $p < 0.0001$ . For two-way ANOVA comparing both treatments and cell lines or clones, statistical significance is indicated by letters, with capital letters (A) for comparing different treatments for the same cell line/clone (e.g., siNeg) and small letters (a) for comparing cell lines/clones for the same treatment (i.e., siNeg versus siACSL4). See also [Figure S4](#).

suggesting that PLA2G6 does not act as a ferroptosis suppressor in the context of PunA-induced ferroptosis. These results strongly suggest that although it may not be sufficient on its own, PLA2G7 may contribute to mitigating PunA-induced ferroptosis in PCa cells, by hydrolyzing the ester bond of PunA-derived hydroperoxides in PLs, thus limiting the propagation of lipid peroxidation at the cell membrane level.

To substantiate our hypothesis that PLA2G7 acts by hydrolyzing PunA-derived PL hydroperoxides (PLOOH), we set up an *in vitro* enzymatic assay based on thin-layer chromatography (TLC) with TMPD detection.<sup>41,42</sup> This method relies on the use of TLC to separate the different hydroperoxide lipid species both from each other and from their parent lipid species (e.g., PLOOH from PL and TG) and on the use of TMPD as a specific hydroperoxide-sensitive spray to visualize the separated hydroperoxides, appearing as purple Wurster spots on the TLC plate while the parent lipid species or alcohols remain unreactive.<sup>43</sup> To test the activity of PLA2G7 on PunA-containing PLOOH, we used PunA-enriched PLs isolated from egg yolks of hens fed a diet rich in pomegranate seed oil for 3 months as starting material<sup>44</sup> and oxidized the PLs into PLOOHs using a photosensitizing agent. TLC-TMPD on PunA-enriched PLOOH revealed a single purple spot with a retention factor corresponding to PLOOH species that was similar to previous reports ([Figure 6L](#)).<sup>43</sup> Upon addition of human recombinant PLA2G7, we observed a marked decrease in the density of the PLOOH purple spot on the TLC plate, as the reaction progressed over time ([Figure 6L](#)). However, we did not observe the appearance of FFA bearing a hydroperoxide function, likely because of the relatively low sensitivity of the method. Of note, we used the same method to test the activity of GPX4 on PunA-enriched PLOOH, as GPX4 reduces PLOOH into alcohols that remain undetected by TMPD.<sup>42</sup> Similarly to PLA2G7, the addition of human recombinant GPX4 protein resulted in a progressive decrease in the density of the PLOOH purple spot over the duration of the enzymatic reaction ([Figure S6K](#)). The abovementioned datasets confirmed that PLA2G7 and GPX4 are capable of removing or reducing, respectively, PunA-derived hydroperoxides from PL species.

**PLA2G7 acts in parallel with GPX4 to protect PCa cells from puni-c-acid-induced ferroptosis**

As individual overexpression of either PLA2G7 or GPX4 was found to have an impact on PunA toxicity but not to be sufficient on its own to fully protect the cells, we investigated whether PLA2G7 would act as a complement to GPX4 in protecting PCa cells from PunA-induced ferroptosis. Indeed, when treated with sublethal doses of both RSL3 and Darapladib, the viability of PunA-treated 22RV1 cells was much more reduced than when treated with PunA and only one of the two inhibitors ([Figure 7A](#)). We thus took a closer look at the relationship between PLA2G7 and GPX4 by silencing either PLA2G7 or GPX4 in 22RV1 cells and treating the cells with PunA and either GPX4 or PLA2G7 inhibitor. The effect of PLA2G7 inhibition by Darapladib on PunA toxicity was significantly amplified in GPX4-silenced cells compared with native 22RV1 cells, with a greater decrease in cell viability ([Figure 7B](#)) and increased level of lipid peroxidation ([Figure 7C](#)). Conversely, PLA2G7 silencing in 22RV1 cells significantly increased the effect of GPX4 inhibition by RSL3 on PunA toxicity, both on cell viability ([Figure 7D](#)) and lipid peroxidation levels ([Figure 7E](#)). These results suggest that PLA2G7 and GPX4 may act complementary to each other to protect 22RV1 cells from PunA-induced ferroptosis. We then overexpressed both PLA2G7 and GPX4 in sensitive PC3 cells and measured the impact of this double overexpression on PunA toxicity. Successful overexpression of both GPX4 and PLA2G7 was confirmed by western blot and RT-qPCR, respectively ([Figures S7A and S7B](#)). The effect of PunA on cell viability and lipid peroxidation levels was completely abolished in PC3 cells overexpressing both PLA2G7 and GPX4 compared with native PC3 cells and PC3 cells overexpressing either GPX4 or PLA2G7 ([Figures 7F and 7G](#)). Importantly, even at a dose of 30  $\mu$ M of PunA, i.e., a dose 10-fold higher than the dose required to kill native PC3 cells, viability, and lipid peroxidation levels in PC3 cells overexpressing GPX4 and PLA2G7 remained similar to untreated cells ([Figures 7F and 7G](#)). On the contrary, when PC3 cells overexpressing both PLA2G7 and GPX4 were treated with RSL3, cell viability and lipid peroxidation levels were comparable to those of GPX4-overexpressing PC3 cells ([Figures S7C and S7D](#)), emphasizing once more the difference between PunA and RSL3 toxicity in PCa cells. Our results thus demonstrate a strong complementary effect between PLA2G7 and GPX4 in limiting PunA-induced lipid

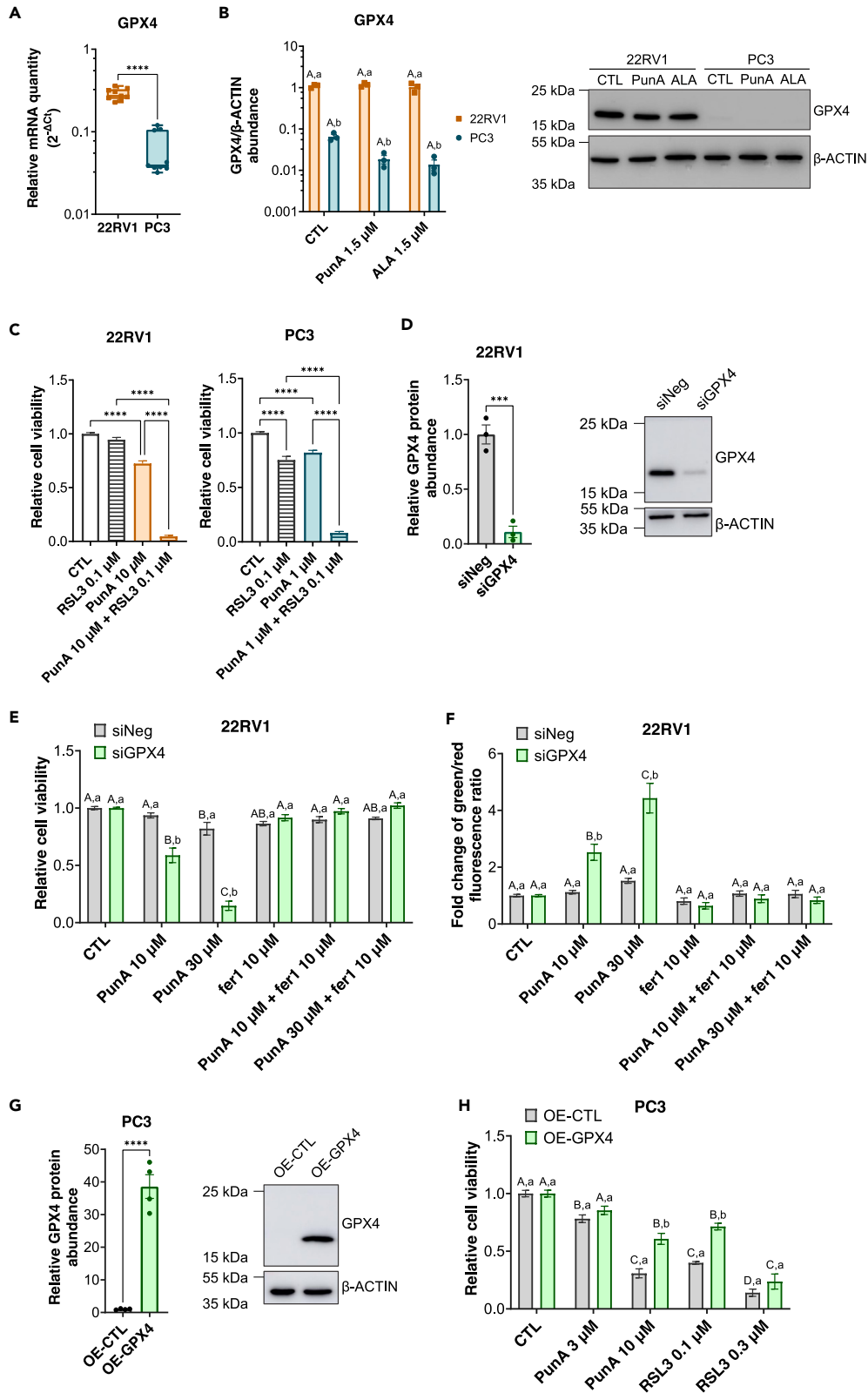


**Figure 5. Sensitivity to puniic-acid-induced ferroptosis partly depends on GPX4 in PCa cells**

(A) Relative mRNA quantity of GPX4 in 22RV1 and PC3 cells, expressed as  $2^{-\Delta\Delta Ct}$  with the geometric mean of the Ct of three reference genes (i.e., GUSB, TBP, and  $\beta$ -ACTIN). Data points represent individual RT-qPCR technical replicates ( $N = 3$ ,  $n = 3$ ).

(B) Ratio of GPX4-to- $\beta$ -ACTIN protein abundance in 22RV1 and PC3 cells treated with either no fatty acid (FA) (control), puniic acid (PunA) 1.5  $\mu$ M, or  $\alpha$ -linolenic acid (ALA) 1.5  $\mu$ M for 24 h. Representative western blot is shown on the right.

(C) Relative viability of 22RV1 and PC3 cells after treatment with either vehicle (DMSO 0.1% v/v, control), RSL3, PunA, or a combination thereof, at the indicated doses, for 24 h, normalized to control.

(D) Relative GPX4 protein abundance of 22RV1 cells transfected with either a negative control siRNA (siNeg) or a siRNA pool targeting GPX4 (siGPX4), normalized to  $\beta$ -ACTIN protein abundance and to siNeg. Representative western blot is shown on the right.

(E) Relative viability of siNeg and siGPX4 22RV1 cells treated with either PunA, ferrostatin-1 (fer1), or a combination thereof for 24 h, normalized to the control (untreated cells).

(F) Lipid peroxidation levels of siNeg and siGPX4 22RV1 cells treated with PunA, fer1, or a combination thereof, at the indicated doses, for 4 h. Data are expressed as the fold change in the green-to-red fluorescence ratio of C11-BODIPY and normalized to control.

(G) Relative GPX4 protein abundance of PC3 cells overexpressing either a negative control vector (OE-CTL) or GPX4 (OE-GPX4), normalized to  $\beta$ -ACTIN protein abundance and OE-CTL. Representative western blot is shown on the right.

(H) Relative viability of OE-CTL and OE-GPX4 PC3 cells treated with either PunA or RSL3 for 24 h, normalized to the control (untreated cells). Data are represented as mean  $\pm$  SEM of  $N \geq 3$  independent cultures (B–H) or as median with the 25–75 percentiles of nine replicates (A). Significance was established by Student's *t* test (A, D, G), one-way ANOVA with Sidak's multiple comparisons (C), or two-way ANOVA with Sidak's multiple comparisons (B, E, F, H). \* $p < 0.05$ , \*\* $p < 0.01$ , \*\*\* $p < 0.001$ , \*\*\*\* $p < 0.0001$ . For two-way ANOVA comparing both treatments and cell lines or clones, statistical significance is indicated by letters, with capital letters (A) for comparing different treatments for the same cell line/clone (e.g., siNeg) and small letters (a) for comparing cell lines/clones for the same treatment (e.g., siNeg versus siGPX4). See also [Figure S5](#).

peroxidation and subsequent ferroptosis in PCa cells. Finally, we measured the abundance of ACSL4, GPX4, and PLA2G7 proteins by western blot in all PCa cell lines for which PunA sensitivity was determined ([Figure 1A](#)). We defined a resistance score for each PCa cell line, i.e., the product of the abundance of GPX4 and PLA2G7 proteins (anti-ferroptotic effect) over the abundance of ACSL4 protein (pro-ferroptotic effect). Interestingly, cell resistance scores strongly correlated with PunA IC50 values, with a Pearson correlation coefficient of 0.93 ( $p$  value = 0.0071) ([Figures 7H](#), [S7E](#), and [S7F](#)). This correlation further highlights the relevant role of the combination of these three proteins in driving PCa cell sensitivity to CLnA-induced ferroptosis.

**DISCUSSION**

Since its discovery a decade ago, ferroptosis has been associated with an increasing number of pathological issues, especially cancer development and aggressiveness.<sup>32</sup> The understanding of the mechanisms underlying ferroptosis has also progressed, with the identification of multiple proteins involved in antioxidant defenses,<sup>6–9,37,45</sup> FA metabolism,<sup>10,30,46</sup> and PL synthesis<sup>47–49</sup> that prevent or promote ferroptosis. At the same time, a growing number of small molecular weight drugs that could effectively and specifically induce ferroptosis has been identified.<sup>32</sup> Yet, another strategy to promote ferroptosis is to exploit cancer cell dependence on taking up considerable amounts of energy precursors from their environment, in particular FAs, as a vulnerability. In the present study, we investigated the mechanisms underlying ferroptosis induced by highly peroxidizable PunA in PCa cells, which are known FA-addicted cancer cells. We showed that PunA is incorporated into specific intracellular lipid species of PCa cells, in particular TGs and PL species. Due to their high potential of peroxidation, PunA acyl chains of PLs are rapidly peroxidized, increasing the intracellular level of lipid peroxides and subsequently leading to ferroptosis in PCa cells ([Figure 8](#)). Although we cannot exclude that other oxidation-dependent cell death pathways, such as oxelptosis,<sup>50</sup> are partly underlying PunA toxicity, our study provides strong evidence that ferroptosis is the major PunA-induced cell death pathway, as we and others have previously demonstrated.<sup>19,21,51</sup> In fact, we speculate that PunA's potential to induce ferroptosis stems from its ACSL4-driven incorporation into specific PL species but not into TGs. Indeed, our results show that blocking TG synthesis rather increases PunA toxicity, which is in line with many previous studies demonstrating the role of lipid droplets as sinks for peroxidizable PUFAs.<sup>18,36,52,53</sup> On the other hand, we have shown that PunA incorporates into PE species, particularly in PC3 sensitive cells, and PEs are known to be more easily peroxidized due to their greater abundance in the inner leaflet of cell membranes,<sup>54</sup> thus playing a major role in driving ferroptosis sensitivity.<sup>12</sup> PunA also led to an overall rise in the ratio of PUFAs to MUFAs in the PLs of PC3 cells, which is consistent with a recent paper proposing this ratio in PLs as a biomarker of cell line sensitivity to ferroptosis.<sup>55</sup> In addition, the ferroptosis inhibitor fer1, which strongly inhibits PunA toxicity, has been shown to function and localize at the level of cell membranes.<sup>56</sup> Another recent study demonstrated that CLnAs do not alter the levels of glutathione, which is water-soluble and cannot trap peroxides in the lipid bilayer, suggesting that CLnAs would indeed rather exert their lethal effects within PLs of cell membranes.<sup>20</sup> Interestingly, our results show that PunA only incorporates into PL species with ester bonds and not with ether bonds, which is in contradiction with a recent study that reported a significant increase in some ether-PE species when cells were treated with  $\beta$ -eleostearic acid, another CLnA isomer.<sup>20</sup> Nevertheless, different CLnA isomers have different double bond configurations and thus steric hindrance, which may lead to different changes in the cellular lipidome.

Although previous studies have already demonstrated the pro-ferroptotic potential of CLnAs in other cancer types, few have focused on the biology underlying their toxicity<sup>21</sup> and none have highlighted a difference in the sensitivity of cancer cell lines of the same tumor type. Here, we report on significant differences in the response of androgen-negative cells and androgen-positive cells to PunA-induced ferroptosis. Importantly, we identified the calcium-independent group VII phospholipase PLA2G7 as a suppressor of PunA-induced ferroptosis, which acts in complement to GPX4 to limit hydroperoxide accumulation in PCa cells. This indicates that the sensitivity of PCa cells to PunA

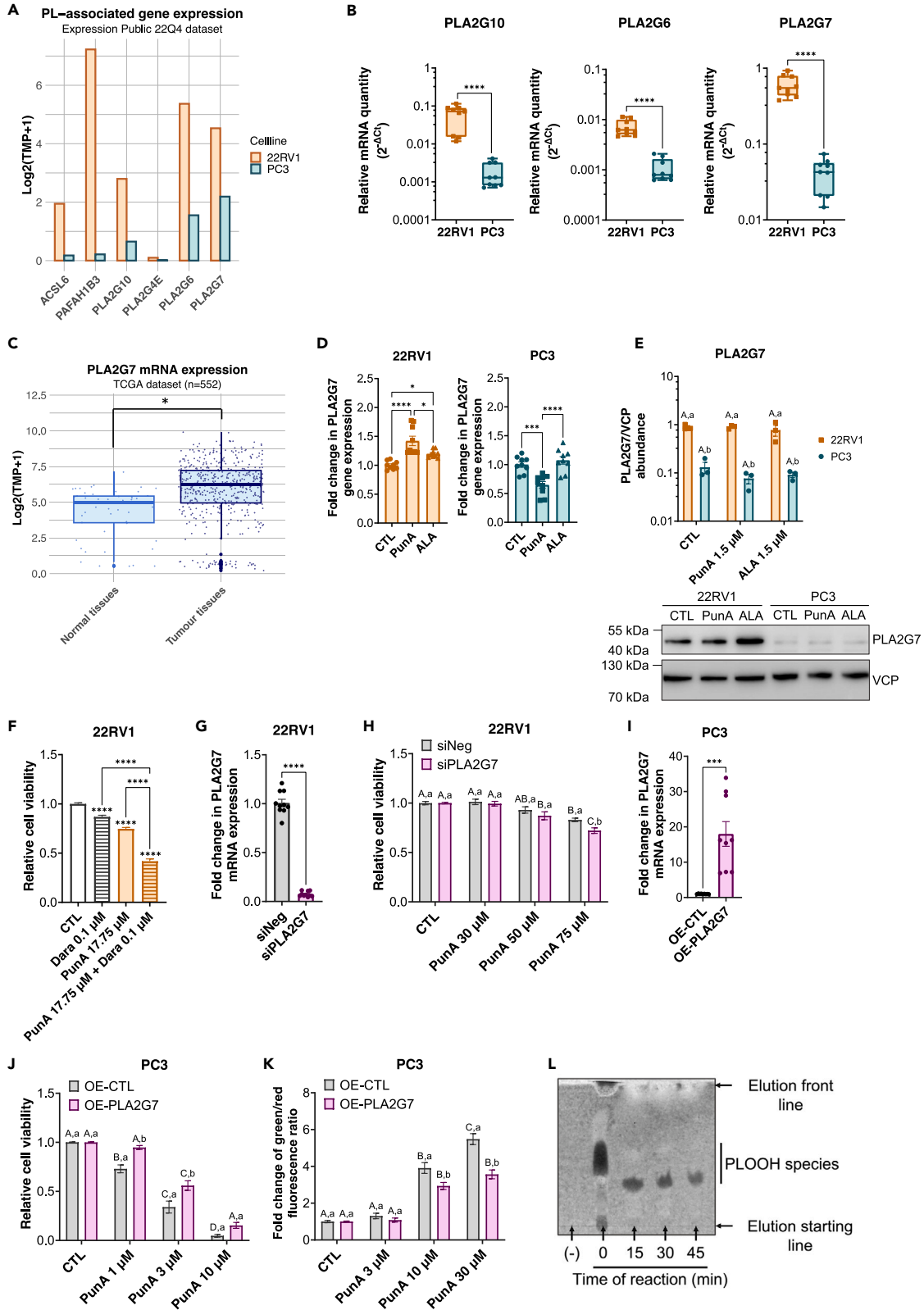


**Figure 6. Phospholipase PLA2G7 is involved in the suppression of puniceic-acid-induced ferroptosis in PCa cells**

- (A) Bar plot of the mRNA expression of PL-related genes from the Expression Public 22Q4 dataset differentially expressed between 22RV1 and PC3 cells. Gene expression is expressed as  $\log_2(\text{TMP}+1)$  from RNA sequencing data.
- (B) Relative mRNA quantity of PLA2G10, PLA2G6, and PLA2G7 in 22RV1 and PC3 cells, expressed as  $2^{-\Delta\text{Ct}}$  with the geometric mean of the Ct of three reference genes (i.e., GUSB, TBP, and  $\beta$ -ACTIN). Data points represent individual RT-qPCR technical replicates ( $N = 3, n = 3$ ).
- (C) Boxplot of the expression of PLA2G7 in normal prostate and prostate tumor tissues from patients of the TCGA cohort. Gene expression is expressed as  $\log_2(\text{TMP}+1)$ . The Limma package was used for Student's t test comparing PLA2G7 mean expression in normal versus tumor tissues. Each data point represents a patient sample.
- (D) Fold change in PLA2G7 gene expression in 22RV1 and PC3 cells treated for 24 h with puniceic acid (PunA) or  $\alpha$ -linolenic acid (ALA) 1.5  $\mu\text{M}$ , normalized to the control (untreated cells). Data points represent individual RT-qPCR technical replicates ( $N = 3, n = 3$ ).
- (E) Ratio of PLA2G7-to-valosin-containing protein (VCP) protein abundance in 22RV1 and PC3 cells treated with either no fatty acid (FA) (control), PunA 1.5  $\mu\text{M}$ , or ALA 1.5  $\mu\text{M}$  for 24 h. Representative western blot is shown below.
- (F) Relative viability of 22RV1 cells after treatment with either vehicle (DMSO 0.1% v/v, control), Darapladib 0.1  $\mu\text{M}$  (Dara), PunA 17.75  $\mu\text{M}$ , or a combination thereof for 24 h. Data were normalized to the control.
- (G) Fold change in PLA2G7 gene expression in 22RV1 cells transfected with either a negative control siRNA (siNeg) or a siRNA pool targeting PLA2G7 (siPLA2G7), normalized to siNeg. Data points represent individual RT-qPCR technical replicates ( $N = 3, n = 3$ ).
- (H) Relative viability of siNeg and siPLA2G7 22RV1 cells treated for 24 h with the indicated doses of PunA, normalized to the control (untreated cells).
- (I) Fold change in PLA2G7 gene expression of PC3 cells overexpressing either a negative control vector (OE-CTL) or PLA2G7 (OE-PLA2G7), normalized to OE-CTL. Data points represent individual RT-qPCR technical replicates ( $N = 3, n = 3$ ).
- (J) Relative viability of OE-CTL and OE-PLA2G7 PC3 cells treated with the indicated doses of PunA for 24 h, normalized to the control (untreated cells).
- (K) Lipid peroxidation levels in OE-CTL and OE-PLA2G7 PC3 cells after 4 h of treatment with the indicated doses of PunA. Data are expressed as the fold change in the green-to-red fluorescence ratio of C11-BODIPY and normalized to the control.
- (L) Representative thin-layer chromatography plate profile of PLOOH species after incubation for 0, 15, 30, or 45 min in the presence of PLA2G7 recombinant enzyme. A control without PLOOH was also added on the plate (corresponding to [–]). Data are represented as mean  $\pm$  SEM of  $N = 3$  independent cultures (D–K) or as median with the 25–75 percentiles of nine replicates (B) or of 552 individual patient samples (C). Significance was established by Student's t test (B, G, H, J, K), one-way ANOVA with Sidak's multiple comparisons (D, F), or two-way ANOVA with Sidak's multiple comparisons (E, I, L, M). \* $p < 0.05$ , \*\* $p < 0.01$ , \*\*\* $p < 0.001$ , \*\*\*\* $p < 0.0001$ . For two-way ANOVA comparing both treatments and cell lines or clones, statistical significance is indicated by letters, with capital letters (A) for comparing different treatments for the same cell line/clone (e.g., siNeg) and small letters (a) for comparing cell lines/clones for the same treatment (e.g., siNeg versus siPLA2G7). See also Figure S6.

depends on the coexpression of ACSL4, GPX4, and PLA2G7. In contrast, PLA2G6 did not appear to be involved in PunA sensitivity, on the contrary to previous studies reporting a significant role of this enzyme as a suppressor of ferroptosis induced by small drugs such as RSL3.<sup>37,38</sup> Similarly, FSP1, which is considered as a major ferroptosis suppressor, particularly in cells lacking GPX4,<sup>8</sup> does not appear to protect PCa cells from PunA-induced ferroptosis. Nevertheless, the role of FSP1 in CLnA-induced ferroptosis requires further investigation. PLA2G7, also known as platelet-activating factor acetylhydrolase (PAF-AH), is an enzyme that catalyzes the hydrolysis of the *sn*-2 ester bond of not only PAF but also PLs containing oxidized fatty acyl groups, typically hydroperoxides.<sup>41,57–59</sup> One of the unifying features of the substrates used by PLA2G7 is their distorted molecular structure, whose formation is expected to deeply alter membrane integrity,<sup>60</sup> as is the case for hydroperoxides in ferroptosis. On the one hand, PLA2G7 has anti-inflammatory properties through the hydrolysis of PAF, a potent inflammatory mediator involved in various inflammatory processes.<sup>58,61,62</sup> On the other hand, PLA2G7 exerts a pro-inflammatory role through the hydrolysis of oxidized PLs, stimulating the development of atherosclerosis.<sup>63</sup> Darapladib, a PLA2G7 inhibitor, has therefore been tested in clinical trials against various pathologies such as atherosclerosis,<sup>63</sup> Alzheimer disease<sup>64</sup> and diabetes,<sup>65</sup> without major success. Here, we propose an additional function for PLA2G7, that is to prevent ferroptosis by releasing hydroperoxides from membrane PLs in PCa cells, as supported by the results obtained via our TLC-based enzymatic assays. PLA2G7 has previously been reported as a potent biomarker of PCa,<sup>66</sup> melanoma<sup>67</sup> and diffuse large B cell lymphoma<sup>68</sup> *in vitro*, *in vivo*, and in cancer patients. Interestingly, PLA2G7 knockdown reduced cell migration and metastasis<sup>66,68</sup> and sensitized ERG-positive PCa cells to oxidative stress.<sup>69</sup> In addition, high PLA2G7 expression in cancer cells was shown to be a potent marker of cancer cachexia in mice and humans with different tumor types.<sup>70</sup> Therefore, targeting PLA2G7, combined with CLnAs, could become a ferroptosis-triggering strategy to prevent cancer progression in PCa patients.

Our results especially highlight the combined effect of PLA2G7 and GPX4 as suppressors of PunA-induced ferroptosis. Although PLA2G7 hydrolyses oxidized PLs and thus removes hydroperoxides from membrane PLs, GPX4 reduces the hydroperoxide group to an alcohol function on PL acyl chains, which can then be hydrolyzed and removed from cell membranes (Figure 8). The ability of PLA2G7 to also hydrolyze PLs with an alcohol function remains to be determined. Yet, another important question in the context of CLnAs is to identify whether PLA2G7 and GPX4 are able to limit the propagation of CLnA-derived peroxidation polymers within cell membranes. In fact, CLnAs have been reported to have peroxidation patterns distinct from those of non-conjugated PUFAs.<sup>22</sup> Whereas non-conjugated PUFAs undergo hydrogen-atom transfer, which leads to the generation of lipid hydroperoxides, conjugated PUFAs can undergo both hydrogen-atom transfer and peroxy radical addition, which leads to the formation of peroxide polymers. It is the additive effect of these two mechanisms that makes CLnAs much more susceptible to autoxidation, in addition to the greater diversity of deleterious aldehydes that are derived from these processes.<sup>20,22</sup> This has been demonstrated for FAs in their free or TG forms. However, whether these polymers can be formed within cell membranes, and whether enzymes such as GPX4 and PLA2G7 are able to reduce or hydrolyze, respectively, these CLnA-derived oxidized PL polymers remains to be investigated.

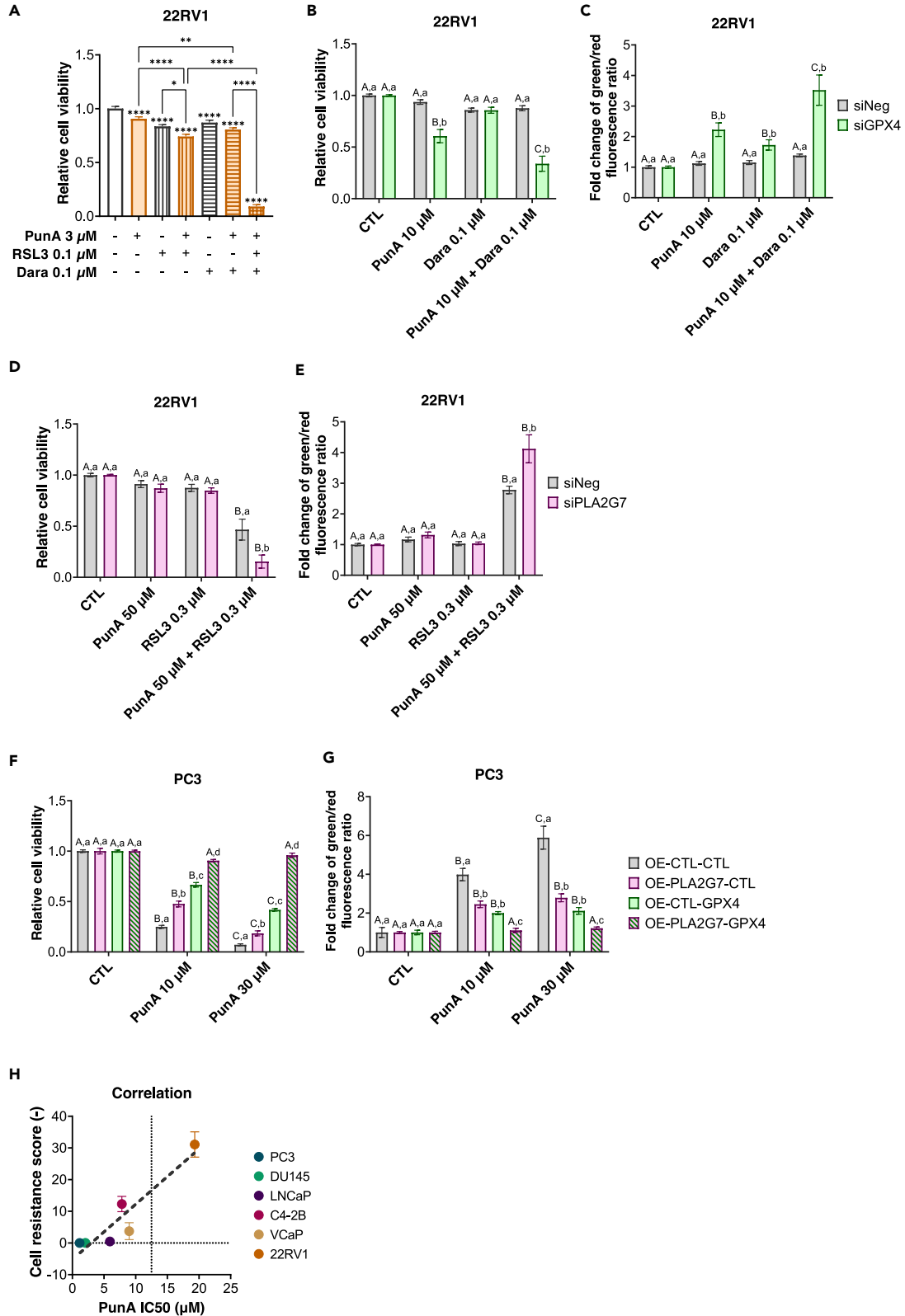


**Figure 7. Phospholipase PLA2G7 acts complementary to GPX4 to protect PCa cells from puniceic-acid-triggered ferroptosis**

(A) Relative viability of 22RV1 cells treated with either vehicle (DMSO 0.1% v/v, control), puniceic acid (PunA) 3  $\mu$ M, Ras-selective lethal (RSL3) 0.1  $\mu$ M, Darapladib (Dara) 0.1  $\mu$ M, or combinations thereof for 24 h, normalized to the control.

(B) Relative viability of 22RV1 cells transfected with either a negative control siRNA (siNeg) or a siRNA pool targeting GPX4 (siGPX4), treated for 24 h with vehicle (DMSO 0.1% v/v, control), PunA 10  $\mu$ M, Dara 0.1  $\mu$ M, or a combination thereof, normalized to the control.

(C) Lipid peroxidation levels in siNeg and siGPX4 22RV1 cells after 4 h of treatment with vehicle (DMSO 0.1% v/v, control), PunA 10  $\mu$ M, Dara 0.1  $\mu$ M, or a combination thereof. Data are expressed as the fold change of the green-to-red fluorescence ratio of C11-BODIPY and normalized to the control.

(D) Relative viability of 22RV1 cells transfected with either a negative control siRNA (siNeg) or a siRNA pool targeting PLA2G7 (siPLA2G7) treated for 24 h with vehicle (DMSO 0.1% v/v, control), PunA 50  $\mu$ M, RSL3 0.3  $\mu$ M, or a combination thereof, normalized to the control.

(E) Lipid peroxidation levels in siNeg and siPLA2G7 22RV1 cells after 4 h of treatment with vehicle (DMSO 0.1% v/v, control), PunA 50  $\mu$ M, RSL3 0.3  $\mu$ M, or a combination thereof. Data are expressed as the fold change of the green-to-red fluorescence ratio of C11-BODIPY and normalized to the control.

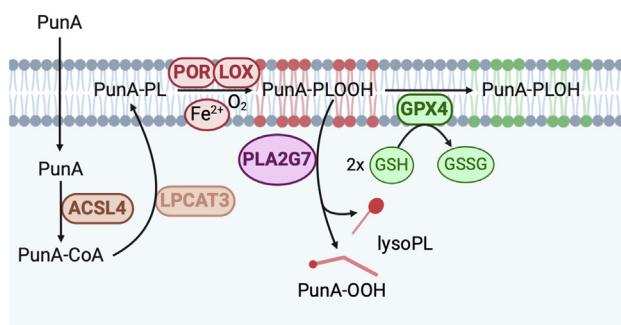
(F) Relative viability of PC3 cells overexpressing either a negative control vector (OE-CTL) or PLA2G7 (OE-PLA2G7) and transfected with either a negative control vector (-CTL) or a GPX4-expressing vector (-GPX4), treated for 24 h with the indicated doses of PunA, normalized to the control (untreated cells).

(G) Lipid peroxidation levels in OE-CTL-CTL, OE-PLA2G7-CTL, OE-CTL-GPX4, and OE-PLA2G7-GPX4 PC3 cells treated for 4 h with the indicated doses of PunA. Data are expressed as the fold change of the green-to-red fluorescence ratio of C11-BODIPY and normalized to the control (untreated cells).

(H) Correlation between the cell resistance score and the PunA IC50 of PC3, DU145, LNCaP, C4-2B, VCaP, and 22RV1 cell lines. Cell resistance score was defined as the product of the abundances of GPX4 and PLA2G7 proteins over the one of ACSL4 protein, determined by western blot and normalized to  $\beta$ -ACTIN (for GPX4 and ACSL4) or valosin-containing protein (VCP) (for PLA2G7) protein abundance. Data are represented as mean  $\pm$  SEM of  $N \geq 3$  independent cultures (A–H). Significance was established by one-way ANOVA with Sidak's multiple comparisons (A) or two-way ANOVA with Sidak's multiple comparisons (B–G). \* $p < 0.05$ , \*\* $p < 0.01$ , \*\*\* $p < 0.001$ , \*\*\*\* $p < 0.0001$ . For two-way ANOVA comparing both treatments and cell clones, statistical significance is indicated by letters, with capital letters (A) for comparing different treatments for the same clone (e.g., OE-CTL-CTL) and small letters (a) for comparing clones for the same treatment (e.g., OE-CTL-CTL vs. OE-CTL-GPX4). See also Figure S7.

CLnAs, particularly if combined with inhibitors of their toxicity regulators such as PLA2G7, may provide an alternative, or at least an adjuvant, to the many ferroptosis-inducing drugs that have proven to be difficult to administer *in vivo*, due to their systemic effects and low stability.<sup>32</sup> The reduction of tumor growth by CLnAs, in particular through the use of Tung oil, rich in the isomer  $\alpha$ -eleostearic acid, has already been reported by others in other tumor contexts.<sup>21,23</sup> Moreover, CLnAs have been shown to be safe for human consumption,<sup>71</sup> and some clinical trials have already reported the absence of adverse effects after taking CLnAs for a few months.<sup>72–75</sup> However, further research is needed to prove the ferroptotic potential of CLnAs from other oils and to determine their most appropriate method of administration *in vivo*. In addition to CLnA-rich oil-based food supplements, an interesting delivery method could be lipid nanoparticles, in the manner of lipid-nanoparticles for mRNA delivery, which have proven to be a highly effective, selective, and stable delivery system.<sup>16,76</sup>

In the present study, we have shown that CLnAs, more specifically PunA, induce ferroptosis in PCa cells, by being incorporated into PL species prone to peroxidation. We identified PLA2G7 as an enzyme capable of removing PunA-derived hydroperoxides from membrane PLs, thereby helping to prevent ferroptosis. Our work also demonstrates that the sensitivity of PCa cells to CLnA-induced ferroptosis depends on the expression of both PLA2G7 and GPX4, which act in a complementary manner to attenuate ferroptosis in PCa cells. Further studies are required to determine the potential of ferroptosis induction with CLnAs and drugs targeting CLnA-induced ferroptosis regulatory mechanisms in PCa tumors *in vivo*.

**Figure 8. Puniceic acid sensitivity of PCa cells relies on both GPX4 and PLA2G7**

Representative scheme of the mechanisms underlying puniceic acid (PunA)-induced ferroptosis sensitivity. PunA is taken up by PCa cells, is activated in its CoA form by ACSL4, and then incorporated into PLs by the action of LPCAT enzymes, such as LPCAT3. Due to autoxidation reactions occurring in the presence of reactive iron and oxygen or the action of specific enzymes such as LOX and POR, PunA acyl chains of PLs (PunA-PL) are peroxidized, leading to the generation of lipid hydroperoxides (PunA-PLOOH). These can be removed from the PLs by the action of PLA2G7, leading to a lysoPL and a free PunA bearing a hydroperoxide function (PunA-OOH). Lipid hydroperoxides can also be reduced into alcohols (PunA-PLOH) by the action of GPX4, relying on the use of GSH. ACSL4, acyl-CoA synthetase 4; ACSL4; POR, cytochrome P450 reductase; GSH, glutathione; GSSG, oxidized glutathione; GPX4, glutathione peroxidase 4; LOX, lipoxygenase; LPCAT3, lysophosphatidylcholine acyl transferase 3; PLs, phospholipids; PLA2G7, calcium-independent group VII phospholipase. Created with BioRender.com.

### Limitations of the study

The present study provides *in vitro* evidence of the ferroptosis-inducing potential of CLnAs and the complementary roles of PLA2G7 and GPX4 in preventing the accumulation of CLnA-derived lipid hydroperoxides at cell membranes. Further studies are necessary to investigate whether there exists a direct interaction between PLA2G7 and GPX4 proteins in PCa cells. Moreover, although the present study emphasizes the mechanisms behind CLnA-induced cell death, further work is needed to study the potential of inducing ferroptosis with CLnAs *in vivo*. Although short-term consumption of CLnAs has been reported to lead to no adverse effects in rodents and humans, ferroptosis induction itself has proven difficult due to significant adverse effects, and there is as yet no consensus concerning its effect on stem cells and immune cells, for instance. Caution should therefore be applied to the use of any molecule that induces ferroptosis, including CLnAs. Although PLA2G7 inhibitor Darapladib has already reached phase III clinical trials in other disease contexts, anti-GPX4 drugs should be used with caution. In addition, *in vivo* studies on CLnAs to date have focused on the use of CLnA-rich vegetable oils, which contain significant amounts of tocopherols, with a strong ferroptosis-inhibiting effect. Further work is thus required to investigate different pharmacological solutions and to find the best formulation for the administration of CLnAs.

### STAR★METHODS

Detailed methods are provided in the online version of this paper and include the following:

- KEY RESOURCES TABLE
- RESOURCES TABLE
  - Lead contact
  - Materials availability
  - Data and code availability
- EXPERIMENTAL MODEL AND STUDY PARTICIPANT DETAILS
  - Cell lines and cell culture
- METHOD DETAILS
  - Fatty acid-BSA complex preparation
  - Cell viability assay
  - Lipid peroxidation detection
  - RNA extraction, reverse transcription and quantitative real-time PCR
  - Immunofluorescence on cells
  - Western blotting and antibodies
  - Fatty acid analysis with GC-FID
  - Generation and quantification of phospholipid hydroperoxides from egg yolk
  - Enzymatic activity assay by thin-layer chromatography
  - Sample preparation and lipidomic analysis with LC-MS
  - Lentivirus production and stable cell line generation
  - Transient gene over-expression
  - Knockdown with small interfering RNA
  - In silico data mining for PLA2G7 identification
- QUANTIFICATION AND STATISTICAL ANALYSIS

### SUPPLEMENTAL INFORMATION

Supplemental information can be found online at <https://doi.org/10.1016/j.isci.2024.109774>.

### ACKNOWLEDGMENTS

We thank Dr. Marcus Conrad for providing us with antibodies against FSP1 and XCT proteins. We warmly thank Eric Mignolet for his relevant thoughts and help in setting up experimental devices. This research was funded by the Foundation Louvain, an Action de Recherche Concertée (ARC 19/24-096) and the F.R.S.- FNRS (Grant 40005227).

### AUTHOR CONTRIBUTIONS

Conceptualization, P.V., O.F., and Y.L.; methodology, P.V., K.G., J.E., and G.L.; experimental work, P.V., K.G., I.N., and M.H.; data analysis and interpretation, P.V., M.M., and M.H.; writing—review & editing, P.V., J.E., G.J., C.D., O.F. and Y.L.; funding and resources, O.F. and Y.L.; supervision, O.F. and Y.L.

### DECLARATION OF INTERESTS

The authors declare that they have no conflict of interest with the content of this article.

Received: November 13, 2023

Revised: March 8, 2024

Accepted: April 15, 2024

Published: April 18, 2024

## REFERENCES

- Dixon, S.J., Lemberg, K.M., Lamprecht, M.R., Skouta, R., Zaitsev, E.M., Gleason, C.E., Patel, D.N., Bauer, A.J., Cantley, A.M., Yang, W.S., et al. (2012). Ferroptosis: An Iron-Dependent Form of Nonapoptotic Cell Death. *Cell* 149, 1060–1072. <https://doi.org/10.1016/j.cell.2012.03.042>.
- Conrad, M., and Pratt, D.A. (2019). The chemical basis of ferroptosis. *Nat. Chem. Biol.* 15, 1137–1147. <https://doi.org/10.1038/s41589-019-0408-1>.
- Agmon, E., Solon, J., Bassereau, P., and Stockwell, B.R. (2018). Modeling the effects of lipid peroxidation during ferroptosis on membrane properties. *Sci. Rep.* 8, 5155. <https://doi.org/10.1038/s41598-018-23408-0>.
- Dai, E., Meng, L., Kang, R., Wang, X., and Tang, D. (2020). ESCRT-III-dependent membrane repair blocks ferroptosis. *Biochem. Biophys. Res. Commun.* 522, 415–421. <https://doi.org/10.1016/j.bbrc.2019.11.110>.
- Seiler, A., Schneider, M., Förster, H., Roth, S., Wirth, E.K., Culmsee, C., Plesnila, N., Kremmer, E., Rådmark, O., Wurst, W., et al. (2008). Glutathione Peroxidase 4 Senses and Translates Oxidative Stress into 12/15-Lipoxygenase Dependent- and AIF-Mediated Cell Death. *Cell Metabol.* 8, 237–248. <https://doi.org/10.1016/j.cmet.2008.07.005>.
- Yang, W.S., SriRamaratnam, R., Welsch, M.E., Shimada, K., Skouta, R., Viswanathan, V.S., Cheah, J.H., Clemons, P.A., Shamji, A.F., Clish, C.B., et al. (2014). Regulation of Ferroptotic Cancer Cell Death by GPX4. *Cell* 156, 317–331. <https://doi.org/10.1016/j.cell.2013.12.010>.
- Bersuker, K., Hendricks, J.M., Li, Z., Magtanong, L., Ford, B., Tang, P.H., Roberts, M.A., Tong, B., Maimone, T.J., Zoncu, R., et al. (2019). The CoQ oxidoreductase FSP1 acts parallel to GPX4 to inhibit ferroptosis. *Nature* 575, 688–692. <https://doi.org/10.1038/s41586-019-1705-2>.
- Doll, S., Freitas, F.P., Shah, R., Aldrovandi, M., da Silva, M.C., Ingold, I., Goya Grocin, A., Xavier da Silva, T.N., Panzilius, E., Scheel, C.H., et al. (2019). FSP1 is a glutathione-independent ferroptosis suppressor. *Nature* 575, 693–698. <https://doi.org/10.1038/s41586-019-1707-0>.
- Soula, M., Weber, R.A., Zilka, O., Alwaseem, H., La, K., Yen, F., Molina, H., Garcia-Bermudez, J., Pratt, D.A., and Birsoy, K. (2020). Metabolic determinants of cancer cell sensitivity to canonical ferroptosis inducers. *Nat. Chem. Biol.* 16, 1351–1360. <https://doi.org/10.1038/s41589-020-0613-y>.
- Doll, S., Proneth, B., Tyurina, Y.Y., Panzilius, E., Kobayashi, S., Ingold, I., Imler, M., Beckers, J., Aichler, M., Walch, A., et al. (2017). ACSL4 dictates ferroptosis sensitivity by shaping cellular lipid composition. *Nat. Chem. Biol.* 13, 91–98. <https://doi.org/10.1038/nchembio.2239>.
- Yuan, H., Li, X., Zhang, X., Kang, R., and Tang, D. (2016). Identification of ACSL4 as a biomarker and contributor of ferroptosis. *Biochem. Biophys. Res. Commun.* 478, 1338–1343. <https://doi.org/10.1016/j.bbrc.2016.08.124>.
- Kagan, V.E., Mao, G., Qu, F., Angeli, J.P.F., Doll, S., Croix, C.S., Dar, H.H., Liu, B., Tyurin, V.A., Ritov, V.B., et al. (2017). Oxidized arachidonic and adrenic PEs navigate cells to ferroptosis. *Nat. Chem. Biol.* 13, 81–90. <https://doi.org/10.1038/nchembio.2238>.
- Ubellacker, J.M., Tasdogan, A., Ramesh, V., Shen, B., Mitchell, E.C., Martin-Sandoval, M.S., Gu, Z., McCormick, M.L., Durham, A.B., Spitz, D.R., et al. (2020). Lymph protects metastasizing melanoma cells from ferroptosis. *Nature* 585, 113–118. <https://doi.org/10.1038/s41586-020-2623-z>.
- Viswanathan, V.S., Ryan, M.J., Dhruv, H.D., Gill, S., Eichhoff, O.M., Seashore-Ludlow, B., Kaffenberger, S.D., Eaton, J.K., Shimada, K., Aguirre, A.J., et al. (2017). Dependency of a therapy-resistant state of cancer cells on a lipid peroxidase pathway. *Nature* 547, 453–457. <https://doi.org/10.1038/nature23007>.
- Hangauer, M.J., Viswanathan, V.S., Ryan, M.J., Bole, D., Eaton, J.K., Matov, A., Galeas, J., Dhruv, H.D., Berens, M.E., Schreiber, S.L., et al. (2017). Drug-tolerant persister cancer cells are vulnerable to GPX4 inhibition. *Nature* 551, 247–250. <https://doi.org/10.1038/nature24297>.
- Zou, Y., Palte, M.J., Deik, A.A., Li, H., Eaton, J.K., Wang, W., Tseng, Y.-Y., Deasy, R., Kost-Alimova, M., Dančik, V., et al. (2019). A GPX4-dependent cancer cell state underlies the clear-cell morphology and confers sensitivity to ferroptosis. *Nat. Commun.* 10, 1617. <https://doi.org/10.1038/s41467-019-09277-9>.
- Yang, W.S., and Stockwell, B.R. (2008). Synthetic Lethal Screening Identifies Compounds Activating Iron-Dependent, Nonapoptotic Cell Death in Oncogenic-RAS-Harboring Cancer Cells. *Chem. Biol.* 15, 234–245. <https://doi.org/10.1016/j.chembiol.2008.02.010>.
- Dierge, E., Debock, E., Guilbaud, C., Corbet, C., Mignolet, E., Mignard, L., Bastien, E., Dessy, C., Larondelle, Y., and Feron, O. (2021). Peroxidation of n-3 and n-6 polyunsaturated fatty acids in the acidic tumor environment leads to ferroptosis-mediated anticancer effects. *Cell Metabol.* 33, 1701–1715.e5. <https://doi.org/10.1016/j.cmet.2021.05.016>.
- Vermond, P., Vancoppenolle, M., Dierge, E., Mignolet, E., Cuvelier, G., Knoops, B., Page, M., Debier, C., Feron, O., and Larondelle, Y. (2021). Punicic Acid Triggers Ferroptotic Cell Death in Carcinoma Cells. *Nutrients* 13, 2751. <https://doi.org/10.3390/nu13082751>.
- Do, Q., Zhang, R., Hooper, G., and Xu, L. (2023). Differential Contributions of Distinct Free Radical Peroxidation Mechanisms to the Induction of Ferroptosis. *JACS Au* 3, 1100–1117. <https://doi.org/10.1021/jacsau.2c00681>.
- Beatty, A., Singh, T., Tyurina, Y.Y., Tyurin, V.A., Samovich, S., Nicolas, E., Maslar, K., Zhou, Y., Cai, K.Q., Tan, Y., et al. (2021). Ferroptotic cell death triggered by conjugated linolenic acids is mediated by ACSL1. *Nat. Commun.* 12, 2244. <https://doi.org/10.1038/s41467-021-22471-y>.
- Do, Q., Lee, D.D., Dinh, A.N., Seguin, R.P., Zhang, R., and Xu, L. (2021). Development and Application of a Peroxyl Radical Clock Approach for Measuring Both Hydrogen-Atom Transfer and Peroxyl Radical Addition Rate Constants. *J. Org. Chem.* 86, 153–168. <https://doi.org/10.1021/acs.joc.0c01920>.
- Dhar Dubey, K.K., Sharma, G., and Kumar, A. (2019). Conjugated Linolenic Acids: Implication in Cancer. *J. Agric. Food Chem.* 67, 6091–6101. <https://doi.org/10.1021/acs.jafc.9b01379>.
- Bray, F., Ferlay, J., Soerjomataram, I., Siegel, R.L., Torre, L.A., and Jemal, A. (2018). Global cancer statistics 2018: GLOBOCAN estimates of incidence and mortality worldwide for 36 cancers in 185 countries. *CA A Cancer J. Clin.* 68, 394–424. <https://doi.org/10.3322/caac.21492>.
- Butler, L.M., Perone, Y., Dehairs, J., Lupien, L.E., de Laat, V., Talebi, A., Loda, M., Kinlaw, W.B., and Swinnen, J.V. (2020). Lipids and cancer: Emerging roles in pathogenesis, diagnosis and therapeutic intervention. *Adv. Drug Deliv. Rev.* 159, 245–293. <https://doi.org/10.1016/j.addr.2020.07.013>.
- Balaban, S., Nassar, Z.D., Zhang, A.Y., Hosseini-Beheshti, E., Centenera, M.M., Schreuder, M., Lin, H.-M., Aishah, A., Varney, B., Liu-Fu, F., et al. (2019). Extracellular Fatty Acids Are the Major Contributor to Lipid Synthesis in Prostate Cancer. *Mol. Cancer Res.* 17, 949–962. <https://doi.org/10.1158/1541-7786.MCR-18-0347>.
- Ahmad, F., Cherukuri, M.K., and Choyke, P.L. (2021). Metabolic reprogramming in prostate cancer. *Br. J. Cancer* 125, 1185–1196. <https://doi.org/10.1038/s41416-021-01435-5>.
- Tousignant, K.D., Rockstroh, A., Taherian Fard, A., Lehman, M.L., Wang, C., McPherson, S.J., Philp, L.K., Bartonicek, N., Dinger, M.E., Nelson, C.C., and Sadowski, M.C. (2019). Lipid Uptake Is an Androgen-Enhanced Lipid Supply Pathway Associated with Prostate Cancer Disease Progression and Bone Metastasis. *Mol. Cancer Res.* 17, 1166–1179. <https://doi.org/10.1158/1541-7786.MCR-18-1147>.
- Tousignant, K.D., Rockstroh, A., Poad, B.L.J., Talebi, A., Young, R.S.E., Taherian Fard, A., Gupta, R., Zang, T., Wang, C., Lehman, M.L., et al. (2020). Therapy-induced lipid uptake and remodeling underpin ferroptosis hypersensitivity in prostate cancer. *Cancer Metabol.* 8, 11. <https://doi.org/10.1186/s40170-020-00217-6>.
- Nassar, Z.D., Mah, C.Y., Dehairs, J., Burvenich, I.J., Irani, S., Centenera, M.M., Helm, M., Shrestha, R.K., Moldovan, M., Don, A.S., et al. (2020). Human DECR1 is an androgen-repressed survival factor that regulates PUFA oxidation to protect prostate tumor cells from ferroptosis. *Elife* 9, e54166. <https://doi.org/10.7554/eLife.54166>.

31. Huo, S., Wang, Q., Shi, W., Peng, L., Jiang, Y., Zhu, M., Guo, J., Peng, D., Wang, M., Men, L., et al. (2023). ATF3/SPI1/SLC31A1 Signaling Promotes Cuproptosis Induced by Advanced Glycosylation End Products in Diabetic Myocardial Injury. *Int. J. Mol. Sci.* **24**, 1667. <https://doi.org/10.3390/ijms24021667>.
32. Stockwell, B.R. (2022). Ferroptosis turns 10: Emerging mechanisms, physiological functions, and therapeutic applications. *Cell* **185**, 2401–2421. <https://doi.org/10.1016/j.cell.2022.06.003>.
33. Feng, H., Schorpp, K., Jin, J., Yozwiak, C.E., Hoffstrom, B.G., Decker, A.M., Rajbhandari, P., Stokes, M.E., Bender, H.G., Csuka, J.M., et al. (2020). Transferrin Receptor Is a Specific Ferroptosis Marker. *Cell Rep.* **30**, 3411–3423.e7. <https://doi.org/10.1016/j.celrep.2020.02.049>.
34. Chen, J., Yang, L., Geng, L., He, J., Chen, L., Sun, Q., Zhao, J., and Wang, X. (2021). Inhibition of Acyl-CoA Synthetase Long-Chain Family Member 4 Facilitates Neurological Recovery After Stroke by Regulation Ferroptosis. *Front. Cell. Neurosci.* **15**, 632354.
35. Wang, Y., Zhang, M., Bi, R., Su, Y., Quan, F., Lin, Y., Yue, C., Cui, X., Zhao, Q., Liu, S., et al. (2022). ACSL4 deficiency confers protection against ferroptosis-mediated acute kidney injury. *Redox Biol.* **51**, 102262. <https://doi.org/10.1016/j.redox.2022.102262>.
36. Jovičić, E.J., Janež, A.P., Eichmann, T.O., Koren, Š., Brglez, V., Jordan, P.M., Gerstmeier, J., Lainšček, D., Golob-Urbanc, A., Jerala, R., et al. (2023). Lipid droplets control mitogenic lipid mediator production in human cancer cells. *Mol. Metabol.* **76**, 101791. <https://doi.org/10.1016/j.molmet.2023.101791>.
37. Chen, D., Chu, B., Yang, X., Liu, Z., Jin, Y., Kon, N., Rabadan, R., Jiang, X., Stockwell, B.R., and Gu, W. (2021). iPLA2 $\beta$ -mediated lipid detoxification controls p53-driven ferroptosis independent of GPX4. *Nat. Commun.* **12**, 3644. <https://doi.org/10.1038/s41467-021-23902-6>.
38. Sun, W.-Y., Tyurin, V.A., Mikulska-Ruminska, K., Shrivastava, I.H., Anthonymuthu, T.S., Zhai, Y.-J., Pan, M.-H., Gong, H.-B., Lu, D.-H., Sun, J., et al. (2021). Phospholipase iPLA2 $\beta$  averts ferroptosis by eliminating a redox lipid death signal. *Nat. Chem. Biol.* **17**, 465–476. <https://doi.org/10.1038/s41589-020-00734-x>.
39. Stremler, K.E., Stafforini, D.M., Prescott, S.M., and McIntyre, T.M. (1991). Human plasma platelet-activating factor acetylhydrolase. Oxidatively fragmented phospholipids as substrates. *J. Biol. Chem.* **266**, 11095–11103.
40. Tew, D.G., Southan, C., Rice, S.Q., Lawrence, M.P., Li, H., Boyd, H.F., Moores, K., Gloger, I.S., and Macphree, C.H. (1996). Purification, properties, sequencing, and cloning of a lipoprotein-associated, serine-dependent phospholipase involved in the oxidative modification of low-density lipoproteins. *Arterioscler. Thromb. Vasc. Biol.* **16**, 591–599. <https://doi.org/10.1161/01.atv.16.4.591>.
41. Kriska, T., Marathe, G.K., Schmidt, J.C., McIntyre, T.M., and Girotti, A.W. (2007). Phospholipase action of platelet-activating factor acetylhydrolase, but not paraoxonase-1, on long fatty acyl chain phospholipid hydroperoxides. *J. Biol. Chem.* **282**, 100–108. <https://doi.org/10.1074/jbc.M608135200>.
42. Kriska, T., and Girotti, A.W. (2005). A thin layer chromatographic method for determining the enzymatic activity of peroxidases catalyzing the two-electron reduction of lipid hydroperoxides. *J. Chromatogr. B Anal. Technol. Biomed. Life Sci.* **827**, 58–64. <https://doi.org/10.1016/j.jchromb.2005.03.045>.
43. Kriska, T., and Girotti, A.W. (2004). Separation and quantitation of peroxidized phospholipids using high-performance thin-layer chromatography with tetramethyl-p-phenylenediamine detection. *Anal. Biochem.* **327**, 97–106. <https://doi.org/10.1016/j.ab.2003.12.021>.
44. Ngo Njembe, M.T., Dormal, E., Gardin, C., Mignolet, E., Debier, C., and Larondelle, Y. (2021). Effect of the dietary combination of flaxseed and Ricinodendron heudelotii or Punica granatum seed oil on the fatty acid profile of eggs. *Food Chem.* **344**, 128668. <https://doi.org/10.1016/j.foodchem.2020.128668>.
45. Mao, C., Liu, X., Zhang, Y., Lei, G., Yan, Y., Lee, H., Koppula, P., Wu, S., Zhuang, L., Fang, B., et al. (2021). DHODH-mediated ferroptosis defence is a targetable vulnerability in cancer. *Nature* **593**, 586–590. <https://doi.org/10.1038/s41586-021-03539-7>.
46. Yamane, D., Hayashi, Y., Matsumoto, M., Nakanishi, H., Imagawa, H., Kohara, M., Lemon, S.M., and Ichi, I. (2022). FADS2-dependent fatty acid desaturation dictates cellular sensitivity to ferroptosis and permissiveness for hepatitis C virus replication. *Cell Chem. Biol.* **29**, 799–810.e4. <https://doi.org/10.1016/j.chembiol.2021.07.022>.
47. Magtanong, L., Ko, P.-J., To, M., Cao, J.Y., Forcina, G.C., Tarangelo, A., Ward, C.C., Cho, K., Patti, G.J., Nomura, D.K., et al. (2019). Exogenous Monounsaturated Fatty Acids Promote a Ferroptosis-Resistant Cell State. *Cell Chem. Biol.* **26**, 420–432.e9. <https://doi.org/10.1016/j.chembiol.2018.11.016>.
48. Zou, Y., Henry, W.S., Ricca, E.L., Graham, E.T., Phadnis, V.V., Maretich, P., Paradkar, S., Boehnke, N., Deik, A.A., Reinhardt, F., et al. (2020). Plasticity of ether lipids promotes ferroptosis susceptibility and evasion. *Nature* **585**, 603–608. <https://doi.org/10.1038/s41586-020-2732-8>.
49. Liang, D., Feng, Y., Zandkarimi, F., Wang, H., Zhang, Z., Kim, J., Cai, Y., Gu, W., Stockwell, B.R., and Jiang, X. (2023). Ferroptosis surveillance independent of GPX4 and differentially regulated by sex hormones. *Cell* **186**, 2748–2764.e22. <https://doi.org/10.1016/j.cell.2023.05.003>.
50. Holze, C., Michaudel, C., Mackowiak, C., Haas, D.A., Benda, C., Hubel, P., Pennemann, F.L., Schnepf, D., Wettmarshausen, J., Braun, M., et al. (2018). Oxeiptosis, a ROS-induced caspase-independent apoptosis-like cell-death pathway. *Nat. Immunol.* **19**, 130–140. <https://doi.org/10.1038/s41590-017-0013-y>.
51. Cuvelier, G., Vermonden, P., Rousseau, J., Feron, O., Rezsöházy, R., and Larondelle, Y. (2023). Resistance to CLnA-induced ferroptosis is acquired in Caco-2 cells upon differentiation. *Front. Cell Death 2*, 1219672.
52. Cruz, A.L.S., Barreto, E.d.A., Fazolini, N.P.B., Viola, J.P.B., and Bozza, P.T. (2020). Lipid droplets: platforms with multiple functions in cancer hallmarks. *Cell Death Dis.* **11**, 105–116. <https://doi.org/10.1038/s41419-020-2297-3>.
53. Petan, T., Jarc, E., and Jusović, M. (2018). Lipid Droplets in Cancer: Guardians of Fat in a Stressful World. *Molecules* **23**, 1941. <https://doi.org/10.3390/molecules23081941>.
54. Doktorova, M., Symons, J.L., and Levental, I. (2020). Structural and functional consequences of reversible lipid asymmetry in living membranes. *Nat. Chem. Biol.* **16**, 1321–1330. <https://doi.org/10.1038/s41589-020-00688-0>.
55. Aldrovandi, M., and Conrad, M. (2020). Ferroptosis: the Good, the Bad and the Ugly. *Cell Res.* **30**, 1061–1062. <https://doi.org/10.1038/s41422-020-00434-0>.
56. Gaschler, M.M., Hu, F., Feng, H., Linkermann, A., Min, W., and Stockwell, B.R. (2018). Determination of the Subcellular Localization and Mechanism of Action of Ferrostatins in Suppressing Ferroptosis. *ACS Chem. Biol.* **13**, 1013–1020. <https://doi.org/10.1021/acscchembio.8b00199>.
57. Stafforini, D.M., and Zimmerman, G.A. (2014). Unraveling the PAF-AH/Lp-PLA2 controversy1. *J. Lipid Res.* **55**, 1811–1814. <https://doi.org/10.1194/jlr.E052886>.
58. Foulks, J.M., Marathe, G.K., Michetti, N., Stafforini, D.M., Zimmerman, G.A., McIntyre, T.M., and Weyrich, A.S. (2009). PAF-acetylhydrolase expressed during megakaryocyte differentiation inactivates PAF-like lipids. *Blood* **113**, 6699–6706. <https://doi.org/10.1182/blood-2008-11-186312>.
59. Stafforini, D.M. (2015). Chapter Six - Plasma PAF-AH (PLA2G7): Biochemical Properties, Association with LDLs and HDLs, and Regulation of Expression. In *The Enzymes Platelet-Activating Factor Acetylhydrolases (PAF-AH)*, K. Inoue, D.M. Stafforini, and F. Tamanoi, eds. (Academic Press), pp. 71–93. <https://doi.org/10.1016/bs.enz.2015.09.004>.
60. Stafforini, D.M. (2009). Biology of platelet-activating factor acetylhydrolase (PAF-AH, lipoprotein associated phospholipase A2). *Cardiovasc. Drugs Ther.* **23**, 73–83. <https://doi.org/10.1007/s10557-008-6133-8>.
61. Xiao, Q., Pepe, A.E., Wang, G., Luo, Z., Zhang, L., Zeng, L., Zhang, Z., Hu, Y., Ye, S., and Xu, Q. (2012). Nrf3-Pla2g7 Interaction Plays an Essential Role in Smooth Muscle Differentiation From Stem Cells. *Arterioscler. Thromb. Vasc. Biol.* **32**, 730–744. <https://doi.org/10.1161/ATVBAHA.111.243188>.
62. Sharma, J., Turk, J., Mancuso, D.J., Sims, H.F., Gross, R.W., and McHowat, J. (2011). Activation of group VI phospholipase A2 isoforms in cardiac endothelial cells. *Am. J. Physiol. Cell Physiol.* **300**, C872–C879. <https://doi.org/10.1152/ajpcell.00289.2010>.
63. Corson, M.A. (2010). Darapladib: an emerging therapy for atherosclerosis. *Ther. Adv. Cardiovasc. Dis.* **4**, 241–248. <https://doi.org/10.1177/1753944710375820>.
64. Maher-Edwards, G., De'Ath, J., Barnett, C., Lavrov, A., and Lockhart, A. (2015). A 24-week study to evaluate the effect of rilapladib on cognition and cerebrospinal fluid biomarkers of Alzheimer's disease. *Alzheimers Dement.* **1**, 131–140. <https://doi.org/10.1016/j.trci.2015.06.003>.
65. Staurengli, G., Ye, L., Magee, M.H., Danis, R.P., Wurzelmann, J., Adamson, P., and McLaughlin, M.M.; Darapladib DME Study Group (2015). Darapladib, a Lipoprotein-Associated Phospholipase A2 Inhibitor, in Diabetic Macular Edema: A 3-Month Placebo-Controlled Study. *Ophthalmology* **122**, 990–996. <https://doi.org/10.1016/j.ophtha.2014.12.014>.
66. Vainio, P., Lehtinen, L., Mirtti, L., Hilvo, M., Seppänen-Laakso, T., Virtanen, J., Sankila, A., Nordling, S., Lundin, J., Rannikko, A., et al. (2011). Phospholipase PLA2G7, associated with aggressive prostate cancer, promotes prostate cancer cell migration and invasion

- and is inhibited by statins. *Oncotarget* 2, 1176–1190.
67. Saenger, Y., Magidson, J., Liaw, B., de Moll, E., Harcharik, S., Fu, Y., Wassmann, K., Fisher, D., Kirkwood, J., Oh, W.K., and Friedlander, P. (2014). Blood mRNA expression profiling predicts survival in patients treated with tremelimumab. *Clin. Cancer Res.* 20, 3310–3318. <https://doi.org/10.1158/1078-0432.CCR-13-2906>.
  68. Zheng, W., Lin, Q., Issah, M.A., Liao, Z., and Shen, J. (2021). Identification of PLA2G7 as a novel biomarker of diffuse large B cell lymphoma. *BMC Cancer* 21, 927. <https://doi.org/10.1186/s12885-021-08660-4>.
  69. Vainio, P., Gupta, S., Ketola, K., Mirtti, T., Mpindi, J.-P., Kohonen, P., Fey, V., Perälä, M., Smit, F., Verhaegh, G., et al. (2011). Arachidonic Acid Pathway Members PLA2G7, HPGD, EPHX2, and CYP4F8 Identified as Putative Novel Therapeutic Targets in Prostate Cancer. *Am. J. Pathol.* 178, 525–536. <https://doi.org/10.1016/j.ajpath.2010.10.002>.
  70. Morigny, P., Kaltenecker, D., Zuber, J., Machado, J., Mehr, L., Tsokanos, F.-F., Kuzi, H., Hermann, C.D., Voelkl, M., Monogarov, G., et al. (2021). Association of circulating PLA2G7 levels with cancer cachexia and assessment of darapladib as a therapy. *J. Cachexia Sarcopenia Muscle* 12, 1333–1351. <https://doi.org/10.1002/jcsm.12758>.
  71. Meerts, I.A., Verspeek-Rip, C.M., Buskens, C.A., Keizer, H.G., Bassaganya-Riera, J., Jouni, Z.E., van Huygevoort, A.H.B.M., van Otterdijk, F.M., and van de Waart, E.J. (2009). Toxicological evaluation of pomegranate seed oil. *Food Chem. Toxicol.* 47, 1085–1092. <https://doi.org/10.1016/j.fct.2009.01.031>.
  72. Khajebishak, Y., Payahoo, L., Alivand, M., Hamishehkar, H., Mobasser, M., Ebrahimzadeh, V., Alipour, M., and Alipour, B. (2019). Effect of pomegranate seed oil supplementation on the GLUT-4 gene expression and glycemic control in obese people with type 2 diabetes: A randomized controlled clinical trial. *J. Cell. Physiol.* 234, 19621–19628. <https://doi.org/10.1002/jcp.28561>.
  73. Mirmiran, P., Fazeli, M.R., Asghari, G., Shafiee, A., and Azizi, F. (2010). Effect of pomegranate seed oil on hyperlipidaemic subjects: a double-blind placebo-controlled clinical trial. *Br. J. Nutr.* 104, 402–406. <https://doi.org/10.1017/S0007114510000504>.
  74. Petrou, P., Ginzberg, A., Binyamin, O., and Karussis, D. (2021). Beneficial effects of a nano formulation of pomegranate seed oil, GranaGard, on the cognitive function of multiple sclerosis patients. *Mult. Scler. Relat. Disord.* 54, 103103. <https://doi.org/10.1016/j.msard.2021.103103>.
  75. Spilmont, M., Léotoing, L., Davicco, M.-J., Lebecque, P., Mercier, S., Miot-Noirault, E., Pilet, P., Rios, L., Wittrant, Y., and Coxam, V. (2013). Pomegranate seed oil prevents bone loss in a mice model of osteoporosis, through osteoblastic stimulation, osteoclastic inhibition and decreased inflammatory status. *J. Nutr. Biochem.* 24, 1840–1848. <https://doi.org/10.1016/j.jnutbio.2013.04.005>.
  76. Kon, E., Ad-El, N., Hazan-Halevy, I., Stotsky-Oterin, L., and Peer, D. (2023). Targeting cancer with mRNA–lipid nanoparticles: key considerations and future prospects. *Nat. Rev. Clin. Oncol.* 20, 739–754. <https://doi.org/10.1038/s41571-023-00811-9>.
  77. Pandeya, A., Li, L., Li, Z., and Wei, Y. (2019). Gasdermin D (GSDMD) as a new target for the treatment of infection. *Medchemcomm* 10, 660–667. <https://doi.org/10.1039/C9MD00059C>.
  78. Smedes, F., and Thomasen, T.K. (1996). Evaluation of the Bligh & Dyer lipid determination method. *Mar. Pollut. Bull.* 32, 681–688. [https://doi.org/10.1016/0025-326X\(96\)00079-3](https://doi.org/10.1016/0025-326X(96)00079-3).
  79. Folch, J., Lees, M., and Sloane Stanley, G.H. (1957). A simple method for the isolation and purification of total lipides from animal tissues. *J. Biol. Chem.* 226, 497–509.
  80. Höring, M., Ejsing, C.S., Hermansson, M., and Liebisch, G. (2019). Quantification of Cholesterol and Cholesteryl Ester by Direct Flow Injection High-Resolution Fourier Transform Mass Spectrometry Utilizing Species-Specific Response Factors. *Anal. Chem.* 91, 3459–3466. <https://doi.org/10.1021/acs.analchem.8b05013>.
  81. Höring, M., Ejsing, C.S., Krautbauer, S., Ertl, V.M., Burkhardt, R., and Liebisch, G. (2021). Accurate quantification of lipid species affected by isobaric overlap in Fourier-transform mass spectrometry. *J. Lipid Res.* 62, 100050. <https://doi.org/10.1016/j.jlr.2021.100050>.
  82. Husen, P., Tarasov, K., Katafiasz, M., Sokol, E., Vogt, J., Baumgart, J., Nitsch, R., Ekroos, K., and Ejsing, C.S. (2013). Analysis of Lipid Experiments (ALEX): A Software Framework for Analysis of High-Resolution Shotgun Lipidomics Data. *PLoS One* 8, e79736. <https://doi.org/10.1371/journal.pone.0079736>.
  83. Liebisch, G., Vizcaino, J.A., Köfeler, H., Trötz Müller, M., Griffiths, W.J., Schmitz, G., Spener, F., and Wakelam, M.J.O. (2013). Shorthand notation for lipid structures derived from mass spectrometry. *J. Lipid Res.* 54, 1523–1530. <https://doi.org/10.1194/jlr.M033506>.
  84. R: The R Project for Statistical Computing <https://www.r-project.org/>.
  85. Josse, J., and Husson, F. (2016). missMDA: A Package for Handling Missing Values in Multivariate Data Analysis. *J. Stat. Software* 70, 1–31. <https://doi.org/10.18637/jss.v070.i01>.
  86. Ahlmann-Eltze, C., and Anders, S. (2019). proDA: Probabilistic Dropout Analysis for Identifying Differentially Abundant Proteins in Label-Free Mass Spectrometry. Preprint at bioRxiv. <https://doi.org/10.1101/661496>.
  87. Ritchie, M.E., Phipson, B., Wu, D., Hu, Y., Law, C.W., Shi, W., and Smyth, G.K. (2015). limma powers differential expression analyses for RNA-sequencing and microarray studies. *Nucleic Acids Res.* 43, e47. <https://doi.org/10.1093/nar/gkv007>.

**STAR★METHODS**

**KEY RESOURCES TABLE**

REAGENT or RESOURCE	SOURCE	IDENTIFIER
<b>Antibodies</b>		
Rabbit monoclonal anti-ACSL4	Abcam	Cat# ab264397 RRID: AB_2714020
Mouse monoclonal anti- $\beta$ -ACTIN	Sigma Aldrich	Cat# A5441 RRID: AB_476744
Rabbit monoclonal anti-DHFR	Cell Signaling Technology	Cat# 45710
Rabbit monoclonal anti-GXP4	Abcam	Cat# ab125066 RRID: AB_10973901
Mouse polyclonal anti-PLA2G6	Santa Cruz antibody	Cat# sc376563 RRID: AB_11150308
Rabbit monoclonal anti-PLA2G7	Abcam	Cat# ab226780
Rabbit monoclonal anti-CD71	Cell Signaling Technology	Cat# 13113 RRID: AB_2715594
Mouse monoclonal anti-VCP	Santa Cruz antibody	Cat# sc57492 RRID:AB_793927
HRP-linked horse anti-mouse IgG	Cell Signaling Technology	Cat# 7076 RRID: AB_330924
HRP-linked goat anti-rabbit IgG	Cell Signaling Technology	Cat# 7074 RRID: AB_2099233
HRP-linked goat anti-rat IgG	Cell Signaling Technology	Cat# 7077 RRID: AB_10496715
Goat anti-rabbit IgG (H+L), Alexa Fluor 555 conjugate	Cell Signaling Technology	Cat# 4413 RRID: AB_10694110
<b>Bacterial and virus strains</b>		
Control expression vector: pLV-Puro-EF1A>ORF_stuffer	VectorBuilder	Cat# VB900122
Control expression vector (transient): pRP-Puro/TagBFP2>ORF_stuffer	VectorBuilder	Cat# VB210619
Envelop plasmid pMD2.G	Addgene	Cat# 12259
GPX4 expression vector: pRP-Puro/TagBFP2>hGPX4	VectorBuilder	Cat# VB900132
Packaging plasmid psPAX2	Addgene	Cat# 12260
PLA2G7 expression vector: pLV-Puro-EF1A>hPLA2G7	VectorBuilder	Cat# VB230505
<b>Chemicals, peptides, and recombinant proteins</b>		
A922500 DAGT1 inhibitor	Sigma Aldrich	Cat# A1737
Adenine	Sigma Aldrich	Cat# A3159
Alpha-linolenic acid	Larodan	Cat# 10-1803
Alpha-Tocopherol	Sigma Aldrich	Cat# T3634
Ammonium tetrathiomolybdate	Sigma Aldrich	Cat# 323446
Apo-transferrin (human)	Sigma Aldrich	Cat# T4382
Arachidonic acid (n-6)	Larodan	Cat# 10-2004
D-Biotin	Sigma Aldrich	Cat# 47868
Bovine Serum Albumin (BSA)	Sigma Aldrich	Cat# A7030

(Continued on next page)

*Continued*

REAGENT or RESOURCE	SOURCE	IDENTIFIER
C11-BODIPY 581/591	Thermo Fisher Scientific	Cat# D3861
Chelex 100 resin	Sigma Aldrich	Cat# C7901
Clarity Max Western ECL substrate	Bio-Rad	Cat# 1705062
Coenzyme Q10	Selleck chemicals	Cat# S2398
Darapladib	Selleck chemicals	Cat# S7520
Deferoxamine mesylate salt	Sigma Aldrich	Cat# D9533
DharmaFECT reagent 2	Dharmacon Horizon	Cat# T-2002-02
DMEM culture medium with L-glutamine	ThermoFisher Scientific	Cat#
DMEM/F12 4:1 culture medium	ThermoFisher Scientific	Cat#
DMSO	Sigma Aldrich	Cat# D5879
Docosahexaenoic acid (n-3)	Larodan	Cat# 10-2206
Docosapentaenoic acid (n-6)	Larodan	Cat# 10-2265
Eicosapentaenoic acid (n-3)	Larodan	Cat# 10-2005
Ethylenediaminetetraacetic acid (EDTA)	Sigma Aldrich	Cat# E6758
Ferostatatin-1	Selleck chemicals	Cat# S7243
Fetal bovine serum	Sigma Aldrich	Cat# F7524
FKGK18	MedChemExpress	Cat# HY115403
L-Glutathione reduced	Sigma Aldrich	Cat# G6013
iFSP1	Selleck chemicals	Cat# S9663
Imidazole Ketone Erastin (IKE)	Selleck chemicals	Cat# S8877
Insulin (human)	ThermoFisher scientific	Cat# 12585-014
Human recombinant GPX4 protein	Cayman chemicals	Cat# 26906
Human recombinant PAFAH protein	Cayman chemicals	Cat# 10279
LDC7559	Selleck chemicals	Cat# S9622
Linoleic acid	Larodan	Cat# 10-1802
Lipofectamine 3000 transfection reagent	Thermo Fisher Scientific	Cat# L3000001
ML210	Selleck chemicals	Cat# S0788
Necrostatin-1	Selleck chemicals	Cat# S8037
Oleic acid	Larodan	Cat# 10-1801
Penicillin/streptomycin 10,000 U/mL	ThermoFisher Scientific	Cat# 15140122
Phosphate Buffer Saline	Sigma Aldrich	Cat# P4417
Polybrene	Sigma Aldrich	Cat# H9268
Presto Blue Reagent	Thermo Fisher Scientific	Cat# A13262
Protease inhibitor cocktail	Sigma Aldrich	Cat# P8340
Punicic acid	Larodan	Cat# 10-1875
Puromycine	InvivoGen	Cat# ant-pr-1
Ras small Lethal 3 (RSL3)	Selleck chemicals	Cat# S8155
Rosiglitazone	Sigma Aldrich	Cat# R2408
RPMI1640 with L-glutamine	ThermoFisher Scientific	Cat# 21875034
N,N,N',N' tetramethyl-p-phenylenediamine	Sigma Aldrich	Cat# T7394
3,3',5-triiodo-L-thyronine	Sigma Aldrich	Cat# T2877
ZVAD-fmk	Selleck chemicals	Cat# S7023

*Critical commercial assays*

Calcium phosphate transfection kit	Sigma Aldrich	Cat# CAPHOS
GoTaq RTqPCR system	Promega Corporation	Cat# A6020

(Continued on next page)

**Continued**

REAGENT or RESOURCE	SOURCE	IDENTIFIER
iScript cDNA synthesis kit	Bio-Rad	Cat# 1708890
MycAlert Mycoplasma Detection kit	Lonza	Cat# LT07
Pierce bicinchoninic acid protein assay	Thermo Fisher Scientific	Cat# A23250
ReliaPrep RNA tissue miniprep system	Promega Corporation	Cat# Z6210

**Experimental models: Cell lines**

Human: 22RV1 cells	DSMZ	Cat# ACC438 RRID: CVCL_1045
Human: C4-2B cells	ATCC	Cat# CRL-3315 RRID: CVCL_4784
Human: DU-145 cells	DSMZ	Cat# ACC261 RRID: CVCL_0105
Human: HEK293T cells	ATCC	Cat# CRL-3216 RRID: CVCL_0063
Human: LNCaP cells	DSMZ	Cat# ACC256 RRID: CVCL_1379
Human: PC3 cells	DSMZ	Cat# ACC465 RRID: CVCL_0035
Human: VCaP cells	ATCC	Cat# CRL-2876 RRID: CVCL_2235

**Oligonucleotides**

ACSL4 ON-TARGETplus Smart pool siRNAs	Dharmacon Horizon	Cat# L-009364-00
GAPDH ON-TARGETplus Smart pool siRNAs	Dharmacon Horizon	Cat# D-001830-10
GPX4 ON-TARGETplus Smart pool siRNAs	Dharmacon Horizon	Cat# L-011676-00
Non-targeting ON-TARGETplus Smart pool siRNAs	Dharmacon Horizon	Cat# D-001810-10
PLA2G6 ON-TARGETplus Smart pool siRNAs	Dharmacon Horizon	Cat# L-009085-00
PLA2G7 ON-TARGETplus Smart pool siRNAs	Dharmacon Horizon	Cat# L-004903-00
See <a href="#">Table S1</a> for primer pairs used in qPCR	This paper	N.A.

**Software and algorithms**

R Studio 4.2.2	Cran R project	<a href="https://cran.r-project.org/bin">https://cran.r-project.org/bin</a>
ImageJ 1.53	ImageJ	<a href="https://fr.vessoft.com/software/windows/download/imagej">https://fr.vessoft.com/software/windows/download/imagej</a>
ALEX	Ejsing Lab	<a href="http://mslipidomics.info/contents/?page_id=133">http://mslipidomics.info/contents/?page_id=133</a>
GraphPad Prism 8.4.2	GraphPad	<a href="https://www.graphpad.com/">https://www.graphpad.com/</a>
Processed lipidomic data	This paper	<a href="https://doi.org/10.14428/DVN/RFGZVW">https://doi.org/10.14428/DVN/RFGZVW</a>
Algorithms for lipidomic data analysis	This paper	<a href="https://zenodo.org/doi/10.5281/zenodo.10796502">https://zenodo.org/doi/10.5281/zenodo.10796502</a>
Expression Public 22Q4 RNA sequencing database	Cancer Cell Line Encyclopedia project	<a href="https://depmap.org/portal/">https://depmap.org/portal/</a>

**RESOURCES TABLE**

**Lead contact**

Further information and requests for resources and reagents should be directed to and will be fulfilled by the lead contact, Yvan Larondelle ([yvan.larondelle@uclouvain.be](mailto:yvan.larondelle@uclouvain.be)).

**Materials availability**

This study did not generate new unique reagents.

### Data and code availability

- Processed lipidomic data have been deposited at [dataverse.uclouvain.be](https://dataverse.uclouvain.be) and are publicly available as of the date of publication. DOI is listed in the [key resources table](#). This paper also analyzes existing, publicly available data. The link to the dataset is listed in the [key resources table](#).
- All original code has been deposited at Zenodo and is publicly available as of the date of publication. DOI is listed in the [key resources table](#).
- Any additional information required to reanalyze the data reported in this paper is available from the [lead contact](#) upon request.

## EXPERIMENTAL MODEL AND STUDY PARTICIPANT DETAILS

### Cell lines and cell culture

Androgen-positive LNCaP, VCaP, C4-2B and 22RV1, and androgen-negative PC3 and DU145 cells were amplified and frozen upon receipt. LNCaP, 22RV1, DU145 and PC3 cell lines were cultured in RPMI1640 culture medium supplemented with 10% fetal bovine serum and 1% of Penicillin/Streptomycin 5000 U/mL. VCaP cells were cultured in DMEM culture medium supplemented with 10% fetal bovine serum and 1% of Penicillin/Streptomycin 5000 U/mL. C4-2B cells were cultured in DMEM/F12 (4:1, v/v) culture medium supplemented with 10% fetal bovine serum, 0.1  $\mu$ g/mL insulin, 275 ng/mL triiodothyronine, 88.6 ng/mL apo-transferrin, 4.9 ng/mL d-Biotin, 252 ng/mL adenine and 1% of Penicillin/Streptomycin 5000 U/mL. Cells were cultured in a humidified incubator at 37°C with 5% CO<sub>2</sub> and were routinely tested negative to *Mycoplasma* contamination using the MycoAlert Mycoplasma Detection kit. All commercially obtained cells were authenticated by the vendors. All compounds were dissolved in DMSO.

## METHOD DETAILS

### Fatty acid-BSA complex preparation

Before being tested on cells, all FAs were conjugated to bovine serum albumin (BSA) in phosphate buffer saline to reach a FA-to-BSA ratio of 4:1 (w/w).

### Cell viability assay

To measure cell viability, cells were seeded at a density of either 10,000 cells/well for PC3 and DU145 cells, 12,000 cells/well for LNCaP and C4-2B cells or 15,000 cells/well for VCaP and 22RV1 cells, respectively, in 96-wells tissue culture treated plates to reach 80% cell confluence. Cells were incubated at 37°C and 5% CO<sub>2</sub> for 24h and then treated with either a FA alone, one or two inhibitor(s) alone or a combination thereof for either 24 or 72h. The doses of the different inhibitors were selected based on previous studies.<sup>8,9,19,21,30,31,77</sup> After 24h or 72h of incubation, cell viability was assessed by using Presto Blue reagent according to manufacturer's instructions.

### Lipid peroxidation detection

Lipid peroxidation was assessed based on the fluorescent lipid probe C11-BODIPY 581/591 (4,4-difluoro-5-(4-phenyl-1,3-butadienyl)-4-bora-3a,4a-diaza-s-indacene-3 undecanoic acid).<sup>19</sup> Upon oxidation, the probe color changes from non-peroxidized (red fluorescence) to peroxidized (green fluorescence). Cells were seeded in a 96-well black/clear bottom plates (Greiner Bio One) and incubated for 24h at 37°C. Cells were then treated with the corresponding treatments (i.e. PunA, fer1, RSL3, Dara, or combinations thereof) for 4h before being incubated with 5  $\mu$ M of C11-BODIPY 581/591 for 30 min at 37°C. Next, cells were washed with PBS and the red and green fluorescence levels were evaluated using a Spectra-max iD3 microplate reader (Molecular Devices) (red:  $\lambda$ excitation = 580 nm,  $\lambda$ emission = 620 nm; green:  $\lambda$ excitation = 500 nm and  $\lambda$ emission = 540 nm). The wavelengths were selected after optimization and spectral range detection. Data are expressed as relative fluorescence units determined by dividing the green fluorescence by the red fluorescence and calculating the ratio between the value obtained for the test condition and the one obtained for the control.

### RNA extraction, reverse transcription and quantitative real-time PCR

Total RNA was extracted and isolated from 22RV1 and PC3 cells using the ReliaPrep RNA tissue miniprep system according to manufacturer's instructions. One  $\mu$ g of RNA for each sample was reverse-transcribed into cDNA with the iScript cDNA synthesis kit. The cDNAs were then amplified by real-time qPCR with the GoTaq RTqPCR system on a StepOne Real Time PCR system (4376357, Thermo Fisher Scientific). The gene expression was calculated via the 2<sup>- $\Delta$ Ct</sup> method and normalized to the geometric mean of reference genes (i.e.  $\beta$ -glucuronidase (GUSB),  $\beta$ -actin ( $\beta$ -ACTIN) and tata-box protein (TBP), which proved to be the best housekeeping genes in PCa cells). The relative gene expression was expressed as fold change in mRNA concentrations compared to the untreated group, which was assigned a value of 1. The primers, which were synthesized and desalted by Eurogentec, are shown in [Table S1](#). All primers were used at a concentration of 300 nM and in a 1/1 forward and reverse ratio, after primer optimization.

### Immunofluorescence on cells

Cells were seeded at a density of 50,000 cells/well or 85,000 cells/well for PC3 or 22RV1 cells, respectively, in a 4-well Lab-Tek Chamber Slide System. Cells were incubated at 37°C and 5% CO<sub>2</sub> for 24h and then treated with either no FA or PunA 30  $\mu$ M for 4h. After incubation, cells were

washed twice with ice-cold PBS and then fixed in PFA 4% for 15 minutes. Cells were then washed three times with PBS before being blocked with 10% w/v skimmed milk in TBS-1% v/v Triton X (TBSTx) for 1h at 4°C. Cells were then incubated overnight at 4°C with an anti-TFR1 antibody (dilution 1/100). After being washed three times with TBSTx, cells were incubated with an Alexa Fluor 555 conjugated anti-rabbit secondary antibody at room temperature for 1h and washed. Finally, nuclei were counterstained with DAPI for 5 minutes and slides were prepared with fluorescence mounting medium (Dako). Stainings were visualized with a Axioskop 2 mot plus fluorescent microscope (Zeiss) and all cell samples were imaged with the same gain and exposure settings for proper comparisons.

The semi-quantification of immunofluorescence pictures was performed using ImageJ 1.53 software. Color channels were split and pictures were inverted. Black zones were defined to cover the fluorescence emission zones on the picture, for both the nuclei and the red fluorescence. The pixel density of the pictures was then measured. The ratio of the pixel densities between TFR1 fluorescence and DAPI was then calculated as the final relative quantification values.

### Western blotting and antibodies

Cells were washed twice with ice-cold PBS and then lysed with home-made RIPA buffer containing 50 mM Tris-HCl at pH 7.4, 150 mM NaCl, 1 mM EDTA, 1% v/v Triton X, 0.05% w/v sodium deoxycholate, 1% w/v SDS and 1% v/v of protease inhibitor cocktail. Protein concentration of cell lysates was measured with the Pierce bicinchoninic acid protein assay. Samples were denatured for 5 minutes at 95°C with Laemmli buffer containing 100 mM dithiothreitol. Twenty µg of proteins for each sample were resolved on SDS-PAGE gels containing 12% v/v acrylamide/bis-acrylamide, and subsequently transferred to a PVDF membrane. Membranes were then blocked with 5% w/v skimmed milk in TBS-0.1% v/v Tween 20 (TTBS) for 1h before being immunoblotted overnight at 4°C with the following specific antibodies: ACSL4 (1:1000), β-actin (1:10,000), DHFR (1:1000), GPX4 (1:1000), PLA2G6 (1:500), PLA2G7 (1:1000) and VCP (1:1000). FSP1 and XCT rat antibodies were kindly gifted by Dr. Marcus Conrad (1:10, Helmholtz Zentrum München, Germany). The specificity of each antibody was first tested on 20 µg of untreated 22RV1 and PC3 cell lysates, without any membrane cutting. After being washed with TTBS, the membranes were incubated with HRP-linked anti-mouse, anti-rat or anti-rabbit antibodies at room temperature for 1h and washed. Membranes were finally revealed using the Clarity Max Western ECL substrate with a chemiluminescence Amersham Imager 600 (Cytiva).

The semi-quantification of Western blot bands was performed using ImageJ 1.53 software. Regions of interest on the blots were selected with the same area of measurement for all bands of a same membrane. The pixel density of each band was measured and inverted by using the “255 – pixel density” formula. The inverted background pixel density was subtracted from each inverted value. The ratio of the pixel densities between the protein of interest and the loading control was then calculated as the final relative quantification values.

### Fatty acid analysis with GC-FID

FA analysis was conducted on preparations of FAs conjugated to BSA to accurately determine their concentrations. FA quantification was also performed on 22RV1 and PC3 cells that were collected 0-2-4-8h post-treatment with PunA 30 µM, and on PC3 cells that were harvested 4h post-treatment with PunA 30 µM, DGAT1 inhibitor 10 µM, Rosiglitazone 10 µM or a combination of PunA and each inhibitor, in order to analyze FA uptake, PunA content and FA profiles of PCa cells. Total lipids were extracted with methanol:chloroform:water (2:2:1; v:v:v) according to the Bligh and Dyer technique.<sup>78</sup> An internal standard composed of nonadecanoic acid (for FFA), 1,2-dipentadecanoyl-sn-glycero-3-phosphatidylcholine (for PL) and triheptadecanoin (for NL), was added in each sample to evaluate extraction yields. Samples were then dried under a stream of nitrogen at 30°C and were methylated under alkaline conditions (0.5 mL of KOH 0.1 M in methanol at 70°C for 1 h) followed by acidic conditions (addition of 0.2 mL of HCl 1.2 M in methanol at 70°C for 15 min). Fatty acid methyl esters (FAMES) were next extracted with 1 mL of hexane. Finally, methyl-undecanoate was added in each sample as an injection standard. FAMES were injected and separated by gas chromatography (Trace 1310) (Thermo Fisher Scientific) equipped with an autosampler TriPlusAS and a RT-2560 capillary column (biscyanopropylpolysiloxane 100 m length, 0.25 mm internal diameter, 0.2 mm film thickness; Restek) flowed with H<sub>2</sub> as carrier gas at a constant pressure of 200 kPa. The GC temperature program was as follows: an initial temperature of 80°C increased to 175°C for 25 min at a rate of 25°C/min, then to 200°C for 20 min at a rate of 10°C/min, then to 220°C for 5 min at a rate of 10°C/min and ultimately at 235°C for 15 min at a rate of 10°C/min. Temperature was finally decreased down to 80°C at a rate of 20°C/min. FAMES were detected with a flame ionizing detector at a constant temperature of 255°C flowed with air (350 mL/min), H<sub>2</sub> (35 mL/min) and N<sub>2</sub> (40 mL/min). An external standard composed of the combination of 43 pure methyl ester standards (Larodan and Nu-Check Prep) was used to identify the unknown peaks with the retention time and to quantify the peaks through the known concentrations. A punicic acid methyl ester standard of known concentration was used to identify and quantify the punicic acid peak in each sample. Chromatograms were processed using ChromQuest 5.0 software (Thermo Fisher Scientific).

### Generation and quantification of phospholipid hydroperoxides from egg yolk

Lipids from PunA-enriched egg yolks were extracted using the Folch procedure.<sup>79</sup> Briefly, 1g of ground egg yolk was extracted with chloroform:methanol (2:1 v/v) using an UltraTurax mixer. The sample was filtered and the filtrate was then mixed with a solution of KCl 0.88% in water in a 5:1 w/w proportion. The upper aqueous phase was removed and water:methanol (1:1 v/v) was added in a 5:1 v/v proportion. After phase separation, the lower organic phase was recovered and evaporated with a rotavapor. Extracted lipids were then resuspended in chloroform to reach a concentration of 100 mg/mL of total lipids.

To isolate phospholipids, 50 mg of fat matter were loaded on solid phase extraction columns (Bond Elut-NH<sub>2</sub>, 1 g, 6 mL) (Agilent Technologies). Neutral lipid, free fatty acid and phospholipid fractions were eluted with chloroform:2-propanol (2:1, v/v), diethyl ether:acetic acid (98:2, v/v) and methanol, respectively. Only the phospholipid fraction was kept for further experiments and was dried under nitrogen flow.

At this stage, part of the sample (i.e. 50  $\mu\text{L}$ ) was analyzed through FA methylation and GC-FID to determine the precise concentration and profile of the PL fraction, as described above. The exact fatty acid profile of the phospholipid fraction from egg yolk is shown in Table S4.

PL hydroperoxides (PLOOH) were generated from isolated PL through photodynamic oxidation by using singlet oxygen-generating ALPcS2 sensitizing agent.<sup>42</sup> PL were diluted at a concentration of 2 mg/mL in chloroform in a 10 mL beaker and were then irradiated in the presence of 5  $\mu\text{M}$  of ALPcS2 for 2h at 4°C with a lamp system covering the UV-A/B and visible light spectrum. After irradiation, samples were aliquoted and dried under nitrogen. Total peroxide content was determined through iodometry. Each sample was dried under nitrogen and dissolved into 0.9 mL of acetic acid:chloroform (3:2, v/v). 20  $\mu\text{L}$  of 0.45 M KI dissolved in demineralized water was added to the sample. The sample was mixed and let for 10 min for the reaction to occur. The absorbance of the triiodide generated from the stoichiometric reaction of iodine with peroxide was measured at 334 nm with a spectrophotometer. Peroxide quantification was based on an extinction coefficient of 22 5000  $\text{M}^{-1}\text{cm}^{-1}$ .<sup>43</sup>

### Enzymatic activity assay by thin-layer chromatography

The activity of GPX4 or PLA2G7 on egg yolk-derived PLOOH was determined by *in vitro* assays followed by thin layer chromatography (TLC).<sup>41,42</sup> Reaction mixtures (0.75 mL) for assessing GPX4 peroxidase activity contained 0.1 mM DFO, 0.1 mM EDTA, 5 mM GSH, 20  $\mu\text{g}/\text{mL}$  rGPX4 and 50  $\mu\text{M}$  PLOOH in Chelex-treated PBS at pH 7.4. Reaction mixtures for assessing lipolytic activity of human recombinant PLA2G7 (or PAFAH) contained 0.1 mM DFO, 0.1 mM EDTA, 0.05% (v/v) Igepal CA-630, 33  $\mu\text{g}/\text{mL}$  of rPLA2G7 and 75  $\mu\text{M}$  of PLOOH in Chelex-treated PBS at pH 7.4. After incubation at 37°C for 15, 30 or 45 minutes, 0.25 mL of samples were removed and extracted with 0.4 mL of ice-cold chloroform:methanol (2:1, v/v). After centrifugation, 0.25 mL of organic phase was recovered and dried under nitrogen.

Samples were then analyzed by TLC with N,N,N',N'-tetramethyl-p-phenylenediamine (TMPD) spray detection. This technique is based on the peroxide-induced oxidation of TMPD to a radical cation chromophore that leads to Wurster purple spots on the TLC plate. Silica-gel 60 TLC plates (10 cm x 20 cm; 0.2 mm layer thickness, Mercks) were dried for 1h at 110°C before use. Dry samples from assay mixtures were resuspended in 20  $\mu\text{L}$  of hexane:ethanol (4:1, v/v) and were applied to a TLC plate. Elution was carried out with chloroform:methanol:acetic acid:water (100:75:7:4, v/v) as mobile phase. Immediately after, the TLC plate was dried with argon and sprayed with a fine mist of freshly prepared 1% (w/v) TMPD in methanol:water:acetic acid (50:50:1, v/v). The TLC plate was dried with argon. When analyte signal appeared maximal relative to background noise (after ~10 minutes), the plate was scanned with an Amersham Imager 600 (Cytiva).

### Sample preparation and lipidomic analysis with LC-MS

Cells were seeded in 6 well-plates and incubated for 24h at 37°C and 5%  $\text{CO}_2$ . Cells were then incubated in the presence of either PunA 2.5–10  $\mu\text{M}$ ,  $\alpha$ -linolenic acid 10  $\mu\text{M}$ , ferostatin-1 (fer1) 10  $\mu\text{M}$  or a combination of PunA 10  $\mu\text{M}$  and fer1 10  $\mu\text{M}$ . After 4h, cells were washed twice with cold PBS and lysed in 1 mL of 0.1% SDS lysis buffer. Protein concentration was measured with the Pierce bicinchoninic acid protein assay. Cell lysates were subjected to lipid extraction according to the method of Bligh and Dyer.<sup>78</sup> An internal standard composed of not naturally occurring lipid species was added as follows: cholesteryl ester (CE) 17:0, CE 22:0, cardiolipin (CL) 14:0/14:0/14:0/14:0, triglyceride (TG) 51:0, TG 57:0, diacylglycerol (DG) 28:0, DG 40:0, ceramide (Cer) d18:1;O2/14:0, Cer d18:1;O2[D7]/18:0, hexosylceramide (HexCer) 18:1;O2/12:0, HexCer 18:1;O2[D5]/18:0, free cholesterol FC[D7], phosphatidylcholine (PC) 14:0/14:0, PC 22:0/22:0, phosphatidyl-ethanolamine (PE) 14:0/14:0, PE 20:0/20:0 (di-phytanoyl), phosphatidylserine (PS) 14:0/14:0, PS 20:0/20:0, phosphatidylinositol (PI) 18:1[D7]/15:0, sphingomyelin (SM) 18:1;O2/12:0, SM 18:1;O2/18:1[D9], lysophosphatidylcholine (LPC) 13:0, LPC 19:0 and lysophosphatidylethanolamine (LPE) 13:0. The chloroform phase was recovered by a pipetting robot (Tecan Genesis RSP 150) and vacuum dried. The residues were dissolved in chloroform/methanol/2-propanol (1:2:4 v/v/v) with 7.5 mM ammonium formate or with 0.005% methylamine (for analysis of CL, HexCer, and PS). Lipids were analyzed using direct flow injection analysis (FIA) on a Fourier-Transform mass spectrometer (FIA-FTMS with high mass resolution).<sup>80,81</sup> The mass spectrometer was equipped with a heated electrospray ionization source and a standard-sized hybrid quadrupole-Orbitrap (Thermo Fisher Scientific). The ion source was operated using a spray voltage of 3.5 kV, S-lens RF level 50, a capillary temperature of 250°C, an aux gas heater temperature of 100°C, and settings of 15 for sheath gas and 5 for aux gas. 50  $\mu\text{L}$  of reconstituted sample extracts were injected by a PAL autosampler (CTC Analytics, Zwingen) equipped with an UltiMate 3000 isocratic pump (Thermo Fisher Scientific). Chloroform/methanol/2-propanol (1:2:4 v/v/v) was delivered at an initial flow rate of 100  $\mu\text{L}/\text{min}$  until 0.25 min followed by 10  $\mu\text{L}/\text{min}$  for 2.5 min and a wash out with 300  $\mu\text{L}/\text{min}$  for 0.5 min. Enhanced Fourier-transform was applied for signal processing. All data were acquired in profile mode. TG, DG and CE were recorded in positive ion mode FTMS in  $m/z$  range 500–1000 for 1 min with a maximum injection time (IT) of 200 ms, an automated gain control (AGC) of  $1 \times 10^6$ , 3 microscans, and a target resolution of 140,000 (at  $m/z$  200). Negative ion mode FTMS data were recorded in  $m/z$  range 400–650 for LPE and LPC and  $m/z$  range 520–960 for PC, PE, PI, PS Cer, HexCer and SM quantification. Cardiolipins were analyzed as [M-H]<sup>-</sup> in negative ion mode  $m/z$  range 1100–1600. Multiplexed acquisition was used for the [M+NH<sub>4</sub>]<sup>+</sup> of free cholesterol (FC) and FC [D7] for 0.5 min acquisition time, with a normalized collision energy of 10%, an IT of 100 ms, AGC of  $1 \times 10^5$ , isolation window of 1  $m/z$ , and a target resolution of 140,000. All FTMS data were processed using the ALEX software,<sup>82</sup> which includes peak assignment and intensity picking. Extracted data were exported to Microsoft Excel and processed by generic macros. The quantification was performed by multiplication of the spiked IS amount with analyte-to-IS ratio. Lipid species were annotated according to the proposal for shorthand notation of lipid structures derived from MS.<sup>83</sup>

All analyses were performed in R (csv4.2.2).<sup>84</sup> Lipid species with a frequency of 70% missing values were filtered out and lipid species abundances were log<sub>2</sub> transformed. To explore the lipidomic data, Principal Component Analysis (PCA) was conducted on all log-transformed lipid species abundances for all cell lines by using the MissMDA R package (version 1.18),<sup>85</sup> to impute the remaining missing values by

regularized iterative PCA algorithm. In order to identify the lipid species whose abundance changes with treatments, Differential Expression Analysis (DEA) was conducted on the abundances of all lipid species for all cell lines by performing a regression with the treatment effect based on the proDA package (version 1.10.0).<sup>86</sup> This method accounts for missing values without imputation by implementing a probabilistic dropout model. Significance was then established with a Wald test on the model coefficient of interest and p-values were adjusted with False Discovery Rate (FDR) for multiple testing.

### Lentivirus production and stable cell line generation

For overexpressing PLA2G7, lentiviruses were collected and packaged from HEK293T cells by co-transfecting a PLA2G7 expression vector or a negative control vector (i.e. ORF\_stuffer, corresponding to a segment of the *E. coli*  $\beta$ -galactosidase gene) with the packaging plasmid and envelop plasmid using the calcium phosphate transfection kit. The supernatants containing the lentiviral particles were harvested 24 h post-transfection and passed through 0.45- $\mu$ m filters. PC3 cells were then incubated with the virus-containing media and 7  $\mu$ g/mL of polybrene for 24h. Following lentiviral infection, PC3 cells containing the expression vectors were selected with 1  $\mu$ g/mL puromycin. PLA2G7 overexpression was detected by both RTqPCR and Western blotting.

### Transient gene over-expression

For transiently overexpressing GPX4, cells were transfected with a GPX4 expression vector or with a negative control vector using Lipofectamine 3000 transfection reagent at a dose of 0.22  $\mu$ L/well for 96-well plates or 5  $\mu$ L/well for 6-well plates. After 24h, culture medium was changed and transfected cells were selected for 24h with puromycin 1  $\mu$ g/mL. After selection, cells were either collected for Western blotting to assess GPX4 expression efficiency or treated with PunA and/or inhibitors (i.e. RSL3, fer1) for another 24h before measuring cell viability.

### Knockdown with small interfering RNA

Cells were transfected with ON-TARGETplus Smart pools targeting ACSL4, GPX4, PLA2G7, PLA2G6, glyceraldehyde-3-phosphate dehydrogenase GAPDH (i.e. positive control) or a non-targeting siRNA pool (i.e. negative control) using DharmaFECT reagent 2. Knockdown efficiency was assessed 72h post-transfection by using Western blotting for ACSL4, GPX4, PLA2G6 and GAPDH or both RTqPCR and Western blotting for PLA2G7. In experiments determining the suppression of PunA toxicity by silencing the expression of GPX4 or PLA2G7, the doses of PunA as well as the ones of RSL3 and Darapladib were selected based on results from cell viability assays.

### In silico data mining for PLA2G7 identification

We explored the Expression Public 22Q4 RNA sequencing database from the Cancer Cell Line Encyclopedia project (<https://depmap.org/portal/>) to investigate the differential expression of genes involved in FA metabolism and phospholipid remodeling between PCa cell lines. Data were downloaded on the DepMap portal, missing values were excluded and the ratio of the gene expression of 22RV1-to-PC3 cells was calculated for each gene. Ratios were filtered out to remove null and infinite values (i.e. corresponding to a division by 0). Ratios > 2 and corresponding to a  $\log_2(\text{TMP}+1)=0.1$  for PC3 gene expression values were arbitrary selected to represent genes with a likely differential expression between cell lines. We then aimed at creating a relevant list of genes by extracting genes from selected molecular signature datasets on the GSEA website (<https://www.gsea-msigdb.org/gsea/msigdb/index.jsp>). The complete list of selected molecular signature datasets is shown in Table S2. The differential expression ratios between PCa cell lines were finally filtered out based on the created list of genes.

We analyzed the differential expression of PLA2G7 in prostate cancer and normal prostate tissues from the Cancer Genome Atlas (TCGA) cohort using the online R2 Genomics Analysis and Visualization Platform (<http://r2.amc.nl>) based on the limma R package.<sup>87</sup>

## QUANTIFICATION AND STATISTICAL ANALYSIS

Statistical analyses were performed through GraphPad Prism 8. Normality of the data was assessed with QQplot of residuals and Shapiro normality tests. Whenever data were not normal, data were log transformed and normality was re-assessed. Statistical analyses were conducted by using either Student's t test, one-way ANOVA with Sidak's multiple comparison test or two-way ANOVA with Sidak's multiple comparison test, when appropriate. Statistical significance is indicated in the Figures as follows: \*p < 0.05; \*\*p < 0.01; \*\*\*p < 0.001; \*\*\*\*p < 0.0001. For two-way ANOVA comparing both treatments and groups (i.e. cell lines or clones from transfection experiments), statistical significance is indicated in the Figures by letters, with capital letters (A) corresponding to comparisons between the different treatments of a same group, and with small letters (a) corresponding to the comparisons between groups of a same treatment. Data are expressed as mean  $\pm$  standard error of the mean (SEM), unless stated otherwise. All experiments were conducted with three independent replicates or more (N  $\geq$  3). When viability data were fitted with dose-response curve, the following equation was used :

$$Y = \text{bottom} + \frac{\text{Top} - \text{bottom}}{1 + \left(\frac{\text{IC50}}{X}\right)^{\text{HillSlope}}}$$

in which all parameters were determined using GraphPad Prism 8.